Available online at www.sciencedirect.com

ScienceDirect

Energy Procedia 63 (2014) 4708 – 4744

Energy Procedia

GHGT-12

Development of improved caprock integrity analysis and risk assessment techniques

Michael S. Bruno[a,*], Kang Lao[a], Julia Diessl[a], Bill Childers[a], Jing Xiang[a], Nicky White[a], Ellen van der Veer[a]

[a]*Geomechancics Technologies, 103 E. Lemon Ave., Suite #200, Monrovia 91016, USA*

Abstract

GeoMechanics Technologies has completed a geomechanical caprock integrity analysis and risk assessment study funded through the US Department of Energy. The project included: a detailed review of historical caprock integrity problems experienced in the natural gas storage industry; advanced coupled transport flow modelling and geomechanical simulation of three large-scale potential geologic sequestration sites to estimate geomechanical effects from large-scale CO_2 injection; and development of a quantitative risk and decision analysis tool to assess caprock integrity risks. Historical data from gas storage operations and CO2 sequestration projects suggest that leakage and containment incident risks are on the order of 10^{-1} to 10^{-2}, which is higher risk than some previous studies have suggested for CO_2. Geomechanical analysis, as described herein, can be applied to quantify risks and to provide operating guidelines to reduce risks. The risk assessment tool developed for this project has been applied to five areas: The Wilmington Graben offshore Southern California, Kevin Dome in Montana, the Louden Field in Illinois, the Sleipner CO_2 sequestration operation in the North Sea, and the In Salah CO_2 sequestration operation in North Africa. Of these five, the Wilmington Graben setting represent the highest relative risk while the Kevin Dome setting represents the lowest relative risk.

Peer-review under responsibility of the Organizing Committee of GHGT-12

*Keywords:*carbon sequestration; caprock integrity; geomechanical modelling; transport flow modelling; risk assessment

* Corresponding author. Tel.: +1-626-305-8460; fax: +1-626-305-8462.
E-mail address: msbruno@geomechanicstech.com

Peer-review under responsibility of the Organizing Committee of GHGT-12
doi:10.1016/j.egypro.2014.11.503

1. Introduction

A primary factor influencing long-term geologic storage of carbon dioxide is caprock integrity. Large-scale CO_2 injection projects require improved and advanced simulation tools and risk assessment techniques to better predict and manage system failures. As part of GeoMechanics Technologies' DOE-funded project, *Development of Improved Caprock Integrity and Risk Assessment Techniques,* we have completed a multi-phase geomechanical caprock integrity study to advance understanding of caprock integrity issues.

First, we provide a review, analysis, and description of historical leakage events related to caprock integrity within the natural gas storage industry. Second, we develop and describe analytical equations that can be applied for first order estimates of induced stresses and strains due to pressure and temperature changes related to CO_2 injection.

Next we describe a process for one-way coupled fluid and heat flow simulation and geomechanical simulation to estimate induced stresses and failure risks. The method has been applied to three potential geologic sequestration sites: the offshore Los Angeles Wilmington Graben; the northern Montana Kevin Dome structure; and the Louden natural gas storage field in central Illinois. Detailed geologic models of each site were created from stratigraphic and lithologic information collected from maps and wells located throughout the fields. The completed geologic models of each of these three sites were used as input for CO_2 injection and fluid migration modelling. To manage areas with uncertain geology, several geologic scenarios were simulated to determine the horizontal and vertical extent of the CO_2 plume after 30 years of injection. Geomechanical models were used to evaluate induced deformations and stresses within the reservoirs and overlying caprocks and to analyze potential fault activation. This paper describes results from our fluid flow and geomechanical modelling for these three potential geologic sequestration sites..

A quantitative risk and decision analysis tool to assess caprock integrity was also developed and applied. Potential loss of caprock integrity is considered due to tensile fracturing, fault activation, and wellbore failure in the caprock. The likelihood of loss events can be assessed in a spreadsheet model for these leakage mechanisms based on a set of general gas-storage and CCS-specific risk factors. For each factor, a range of parameter values associated with high, moderate and low leakage risk conditions is evaluated and assigned an order of magnitude relative score. This leads to a total score of each set of site-specific parameter values, which can be translated into a loss event probability. The relative risk ranking tool is described herein, and applied to the three potential sequestration sites, and to two historical large scale sequestration projects, providing their relative risk.

2. Review of historical caprock integrity problems experienced in the natural gas storage industry, with implications for CO_2 leakage incident probability

2.1. Underground Storage of Natural Gas

Natural gas is stored underground primarily in depleted oil and gas reservoirs, saline aquifers, and solution mined salt caverns to help meet cyclic seasonal demands for gas. It is a practice that reduces price volatility and balances the flow in pipeline systems [1 & 9]. In seasonal storage, natural gas is injected during the summer, when demand for heating is low, and is withdrawn during the winter season. Depleted gas reservoirs and saline aquifers are both used for this type of storage. Salt caverns are used for short-term storage, because they can quickly switch from injection to withdrawal and operate at large injection and extraction rates [1].

The practice of underground natural gas storage can provide useful insights related to risk assessment for geologic storage of CO_2. Although CO_2 and CH_4 have different density and solubility, this type of operation is more directly relevant to geologic storage than other waste injection operations because, like CO_2, natural gas is less dense than water and consequently will behave as a buoyant fluid. They also have similar viscosity, and anticipated CO_2 injection rates are comparable to current CH_4 injection rates [6].

There are currently more than 400 underground storage sites in the United States and more than 100 storage sites in Europe and Central Asia (see for example Fig.1 and Fig.2). About 80% of these are in depleted oil and gas fields, with the remainder approximately evenly divided between saline aquifers and solution mined salt caverns [4 & 5].

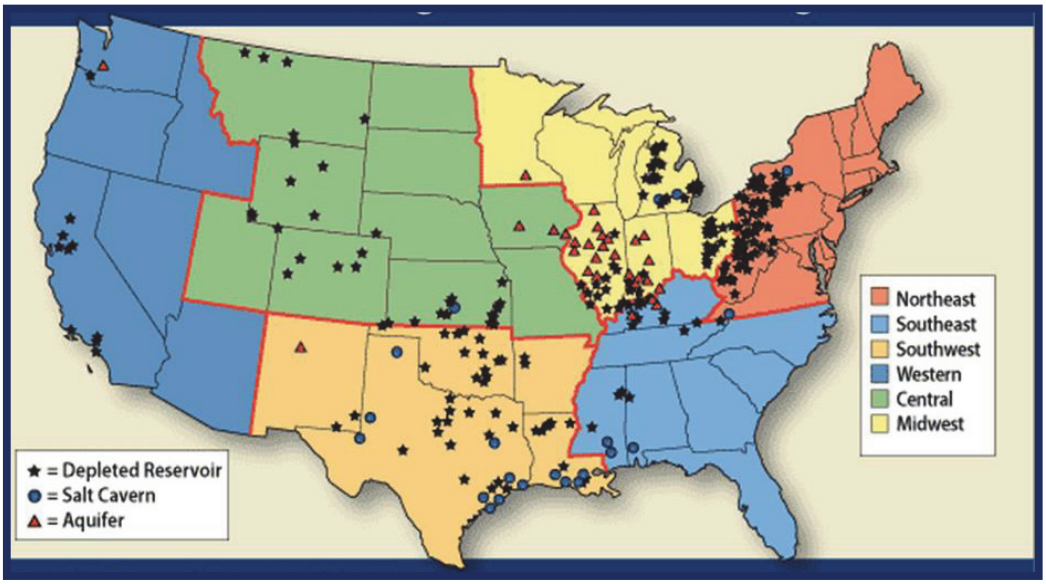

Fig.1. U.S. Underground Natural Gas Storage Facilities [11].

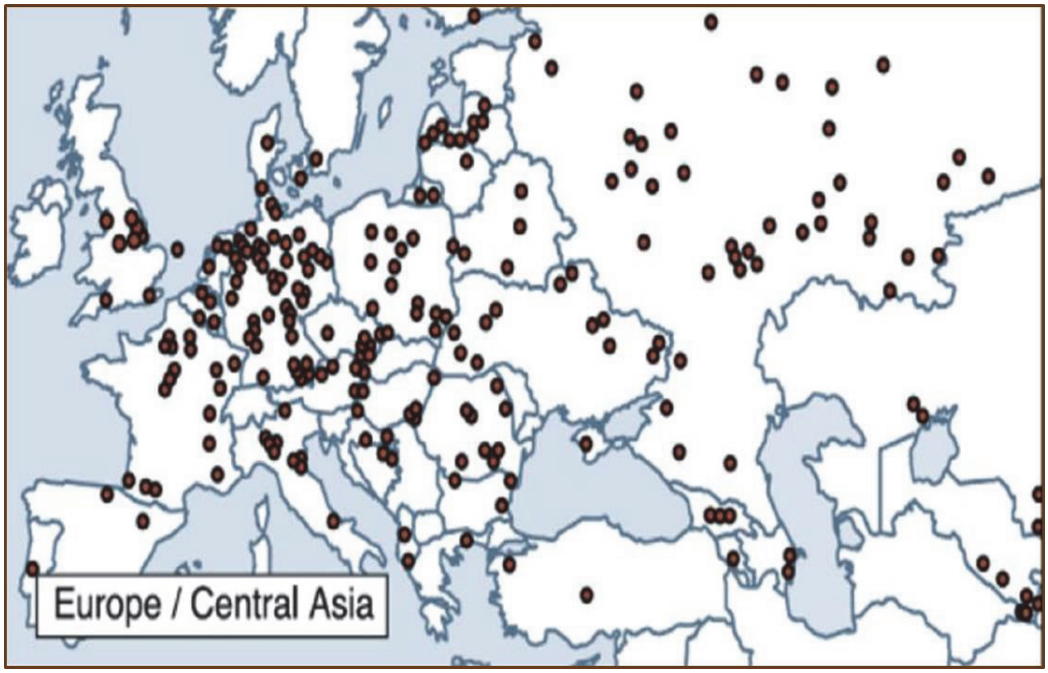

Fig.2. Underground Natural Gas Storage Facilities in Europe and Central Asia (IEAGHG, 2009).

The necessary conditions for underground natural gas storage are similar to those for CCS [1]. These are:

- A geologic structure under in which fluid can be trapped (e.g., an anticline with sufficient closure);
- A reservoir (i.e., porous and permeable layers of rock);
- A caprock (i.e., impermeable or low-permeable, water-wet rock layers that prevent the stored fluid from rising or moving laterally to rise elsewhere);
- Water present to confine the stored fluid in all directions; and,
- Adequate overburden (depth) to allow the storage of fluids under sufficiently high pressures.

In addition to natural gas storage, other industries utilizing these same conditions for injection operations include oil and gas waste disposal (for both liquids and solids), industrial hazardous and non-hazardous waste disposal, and municipal sanitation waste disposal. (See for example: Benson [1], IPCC [2], Perry [3], EIA [4 & 5], Lewicki et al. [6], Burton et al. [7], Myer [8], and DNV [9]).

2.2. Caprock Integrity Problems and Gas Leakage Incidents

Natural gas storage fields are operated around the world, and the majority of these operate without problems. In some instances, however, gas has migrated from the storage zone to overlying and/or adjacent formations, to shallow groundwater, and even to the surface. Although most of these instances are related to well integrity problems, some have occurred due to caprock integrity failure. So far there are no documented cases of fully remediating a leak in a caprock in either a natural gas storage or waste injection project [7]. Performing such remediation work in the future is speculative at best. For the most part, these leaks could have been avoided through proper and thorough geologic characterization of the caprock.

We have reviewed historical data and documented caprock integrity problems in the gas storage industry. Reviewing and analyzing many of these incidents provides useful information to the CO_2 sequestration industry, helping to recognize and identify risk conditions and improve project design and operating practices to help ensure permanent geologic storage. This effort consisted in collecting and analyzing gas storage data associated with caprock integrity problems, and examining maximum pressure limits and analyzing past failure incidents that have occurred during gas storage operations.

Relying principally on two previous studies [3 & 10], we identified 22 incidents of gas leakage due to caprock integrity issues worldwide, about 10% of all reported leakage incidents. Of these, half were due solely to an insufficiently gas-tight caprock, whether too thin, too permeable, or made of dissoluble constituents. Another quarter of these incidents were due solely to undetected or incorrectly characterized faults and/or fractures through the caprock, allowing fluid communication between the reservoir and formations unintended for storage. Finally, the remaining quarter was cases in which both of these factors are believed to have played a role in leakage.

It should come as no surprise that most instances of these *geologically related* gas migration problems have occurred in aquifer gas storage operations. While comprising only about 10% of natural gas storage reservoirs overall, aquifer storage operations account for about 65% of these 22 incidents. In some cases the flaws in the caprock were associated with previously unrecognized fracturing or faulting associated with the anticlinal structure of the gas storage field. Typically, a large anticlinal structure with as many feet of closure as possible is an important criteria for an aquifer gas storage field (see **Error! Reference source not found.**). Large structural deformation, however, introduces a greater possibility of caprock flaws and potential leakage [3].

The two root causes for failures for many of these, and likely for all of these 22 cases, are because the geology of the site was not properly characterized and/or the pressure in the storage reservoir was too high [1].

Creating pressure gradients that the storage formations have not experienced before can result in the displacement of the static water column, forcing water out of the cap rock and causing gas to leak from the storage formation [12],

thus exceeding the threshold displacement pressure or threshold pressure (i.e., the gas pressure is high enough to displace water-gas menisci in the rock pores) [1].

It is also important to recognize that the pressure required to fracture a reservoir is not constant, but changes with average reservoir pressure. It is easier to fracture a formation that is in a pressure depleted state as compared to the reservoir at original pressure conditions.

The majority geologically related leakage incidents have occurred in saline aquifers converted to gas storage. In these cases, conduits in the caprock occur due to fracturing or faulting associated with anticlinal structures. Leaks occur as a result of the more challenging nature of aquifer gas storage: less geologic data, higher required pressures and unconfirmed sealing.

To estimate failure rates and risk, several researchers have documented incidents of leakage at UNGS facilities. Based on our survey of these studies, the rate of failure can be estimated: of 485 operational and abandoned UNGS facilities in the U.S., Europe and Central Asia, 39 of these reservoirs have experienced leakage representing an 8% incident rate. For example, Table 1 below provides a summary of reported observations by Evans (2009).

Table 1 Summary of gas storage leakage incidents reported by Evans (2009)

U.S. UGS Leakage Events:

Contributory processes/mechanisms attributed to leakage/failure	Storage Facility Type		
	O&G Fields	Aquifers	Totals
Migration from Injection Footprint/Cavern (not Due Entirely to Well Problems)	11	13	24
Caprock - Not Gas Tight/Salt Thick Enough	**3**	**12**	**15**
Caprock - Fractured/Faulted, Not Gas-Tight	**4**	**5**	**9**
Seismic Activity	1	0	1
Not Available	4	1	5

• ~373 US UNGS facilities operational and abandoned in O&G fields and aquifers

• 28 of these reservoirs have experienced leak incidents

• 28/373 = 7.5% incident rate

European UGS Leakage Events:

Storage Facility Type					
Country	Depleted field	Aquifer	Salt Cavern	Mine/ Rock Cavern	Total
Russia			6		6
France		1	3		4
Germany	1	4	2		7
Poland		1			1
Hungary		1			1
Belgium				1	1
Denmark		1			1
Finlang				1	1
GB&Ireland	2		1		3
Sum	**3**	**8**	**12**	**2**	**25**

• ~112 European UGS facilities operational and abandoned in O&G fields and aquifers

• 11 of these reservoirs have experienced leak incidents

• 11/112 = 9.8% incident rate

It is very important to recognize, however, that reported and documented leakage incidents are not at all comprehensive. Most leakage incidents are not documented. During the past five years GeoMechanics Technologies has been involved in half a dozen legal disputes involving storage gas migration which are not documented or mentioned in literature. The natural gas storage industry has a strong economic incentive not to lose gas. Yet it does not achieve anything close to 99% containment over decades, the stated goal of some organizations such as the US Department of Energy Geologic Storage Program. In our opinion 99% containment over 100 years is a worthy goal, but not a likely outcome.

Based on historical data from the gas storage industry, and even based on recent experience with large scale CO_2 sequestration projects to date (consider In Salah for example), a one in ten (10^{-1}) probability of out of zone leakage incidents is a reasonable order of magnitude estimate for leakage risk with CO_2 sequestration projects. That is, of every 10 large scale CO_2 sequestration projects, expect that one or more will experience out of zone leakage incidents. But it is also important to note that leakage out of zone does not generally result in leakage to surface. Reservoir and overburden geologic and geomechanical characterization is a critical requirement for risk assessment.

3. Analytical equations for first order estimates of induced stresses and strains caused by CO_2 injection

Injection of large quantities of CO2 into a porous media necessarily requires elevation of the pore pressure in order to displace the existing fluids. Large scale CO2 injection also modifies temperature, as injected material is generally lower temperature than the formation. These pressure and temperature changes in the storage zone cause formation expansion and induce stresses in the overlying caprock. The geomechanical integrity of the caprock can be compromised by three basic mechanisms. These are:

1. Potential tensile fracturing;
2. Potential fault activation;
3. Potential bedding plane slip.

In general the stresses induced in the caprock and resulting damage risk must be determined through 3D geomechanical modelling and numerical simulation. It is important, however, to consider the underlying physics and fundamental analytical solutions upon which such analyses are based, in order to gain insight into the important mechanisms and parameters which influence caprock integrity.

If we consider a small volume element V within the storage zone, the change in volume ΔV induced by pressure and temperature changes may be expressed as:

$$\Delta V/V = Cb\Delta P + 3\alpha\Delta T \quad (1)$$

where Cb is the material bulk compressibility and α is the linear coefficient of thermal expansion. Note that both pressure increase and temperature increase induce expansion. Conversely, a pressure decrease and a temperature decrease induce contraction.

If the storage formation was completely free to expand or contract in all directions, there would be no stresses induced. The surrounding formations, however, constrain this deformation. The result is that stresses are induced both within the storage reservoir and within the surrounding material (including the caprock). Considering only pore pressure increase, for example, compressive stresses are induced within the storage zone and tensile and shear stresses are induced in the caprock. These can lead to one or several of the caprock failure mechanisms listed above.

To further illustrate and discuss this fundamental mechanism inducing stresses in the caprock, we consider the displacements that are induced in the surrounding formation due to a center of dilation or contraction within the storage zone. As a first approximation, we describe and consider the fundamental equations for displacements, strains, and stresses in a continuum. Using index notation, strains ε_{ij} are related to displacement gradients $u_{i,j}$ through the equations:

$$\varepsilon_{ij} = \frac{1}{2}\left(u_{i,j} + u_{j,i}\right) \quad (2)$$

For general elasticity, the stresses in a body σ_{ij} are related to the strains through a general stiffness matrix C_{ijkl} and tensor relationship as follows:

$$\sigma_{ij} = C_{ijkl}\varepsilon_{kl} \quad (3)$$

The number of independent material properties contained in the stiffness relations of equation (3) depends on the type of material behavior. For completely “isotropic” materials (in which stiffness properties do not vary in any

direction), there are only two independent material properties. Sedimentary formations are typically "transversely isotropic". That is, stiffness properties are constant in both directions parallel to bedding, but different in a direction perpendicular to bedding. For such materials, there are five independent material properties. But sedimentary layers with vertical fracture will have different stiffness properties even in the two directions parallel to bedding. Such materials are called "orthotropic", and contain nine independent material properties. Considering the simplest case of isotropic materials, the stress-strain and stress-displacement relations can be expressed as follows:

$$\sigma_{ij} = \lambda\delta_{ij}\varepsilon_{kk} + 2G\varepsilon_{ij} = \lambda\delta_{ij}u_{i,j} + G\left(u_{i,j} + u_{j,i}\right) \tag{4}$$

where λ and G are two independent material properties and δ_{ij} is the Kronecker delta which takes a value of unity when i=j and a value of zero otherwise. The material properties λ and G are can be expressed in terms of the more commonly used Young's Modulus, E, and Poisson's Ratio ν, through:

$$\lambda = \frac{\nu E}{(1+\nu)(1-2\nu)} \quad \text{and} \quad G = \frac{E}{2(1+\nu)} \tag{5}$$

Equation (4) can be applied to estimate the stresses induced in the caprock if the strains or displacement field is known. Solutions for the displacements and stresses induced in a half-space due to a center of dilation (or contraction) have been presented by Sen (1950) and Geertsma (1973) and applied by a number of researchers to evaluate subsidence and casing deformations induced by compacting reservoirs (see for example Bruno et al, 1998 [34]; Bruno, 2002 [35]). The displacement field produced by a center of dilation located at position (x_o, y_o, z_o) with pressure and temperature change, as given in Equation (1), is provided by the set of equations below:

$$u_x = P\left[\frac{\partial V_1}{\partial x} + 2z\frac{\partial^2 V_2}{\partial x\,\partial z} + (3-4\nu)\frac{\partial V_2}{\partial x}\right] \tag{6}$$

$$u_y = P\left[\frac{\partial V_1}{\partial y} + 2z\frac{\partial^2 V_2}{\partial y\,\partial z} + (3-4\nu)\frac{\partial V_2}{\partial y}\right] \tag{7}$$

$$u_z = P\left[\frac{\partial V_1}{\partial z} + 2z\frac{\partial^2 V_2}{\partial z^2} - (3-4\nu)\frac{\partial V_2}{\partial z}\right] \tag{8}$$

Where,

$$P = \frac{(1+\nu)}{12\pi(1-\nu)}\left[C_b\,\Delta P + 3\alpha\Delta T\right] \tag{9}$$

$$V_1 = \left[(x-x_0)^2 + (y-y_0)^2 + (z-z_0)^2\right]^{-\frac{1}{2}} \tag{10}$$

$$V_2 = \left[(x-x_0)^2 + (y-y_0)^2 + (z+z_0)^2\right]^{-\frac{1}{2}} \tag{11}$$

Equations (4) may now be combined with equations (6) through (11) to determine the stresses induced in the caprock due to pressure and temperature changes occurring within the storage zone. This is valid for elastic behavior of isotropic materials. For example, the horizontal shear stresses induced in the caprock, which might lead towards bedding plane slip and well damage, can be expressed as:

$$\sigma_{xz} = G\left[{}^{\partial u_x}/_{\partial z} + {}^{\partial u_z}/_{\partial x}\right] = \frac{EP}{(1+\nu)}\left[\frac{\partial^2 V_1}{\partial x\,\partial z} + 2z\frac{\partial^3 V_2}{\partial x\,\partial z^2} + \frac{\partial^2 V_2}{\partial x\,\partial z}\right] \tag{12}$$

and,

$$\sigma_{yz} = G\left[{}^{\partial u_y}/_{\partial z} + {}^{\partial u_z}/_{\partial y}\right] = \frac{EP}{(1+\nu)}\left[\frac{\partial^2 V_1}{\partial y\,\partial z} + 2z\frac{\partial^3 V_2}{\partial y\,\partial z^2} + \frac{\partial^2 V_2}{\partial y\,\partial z}\right] \tag{13}$$

Similar equations can be developed for any of the stress components at any location within the caprock. The change in pressure and temperature is measured from some reference state (typically the initial reservoir conditions) from which induced stresses are to be determined. The total induced stresses caused by varying temperature and pressure fields within an arbitrarily shaped reservoir can be obtained by integrating the contribution of all the center of dilation points over the entire reservoir volume. The equations above may be integrated analytically if the pressure and temperature distribution and reservoir shapes are simple functions, or numerically if they are more complex.

To illustrate a typical distribution of shear stresses within the caprock at the top of a reservoir, we present parametric results from numerical integration of equations (12) and (13) for an axisymmetric reservoir volume of radius R and height H, located at depth d below the surface, in which pressure change varies linearly from a maximum of ΔP at r=0 to zero at r=R. Shear stresses in figure 3 are normalized with respect to reservoir radius, height, pressure change, and material properties.

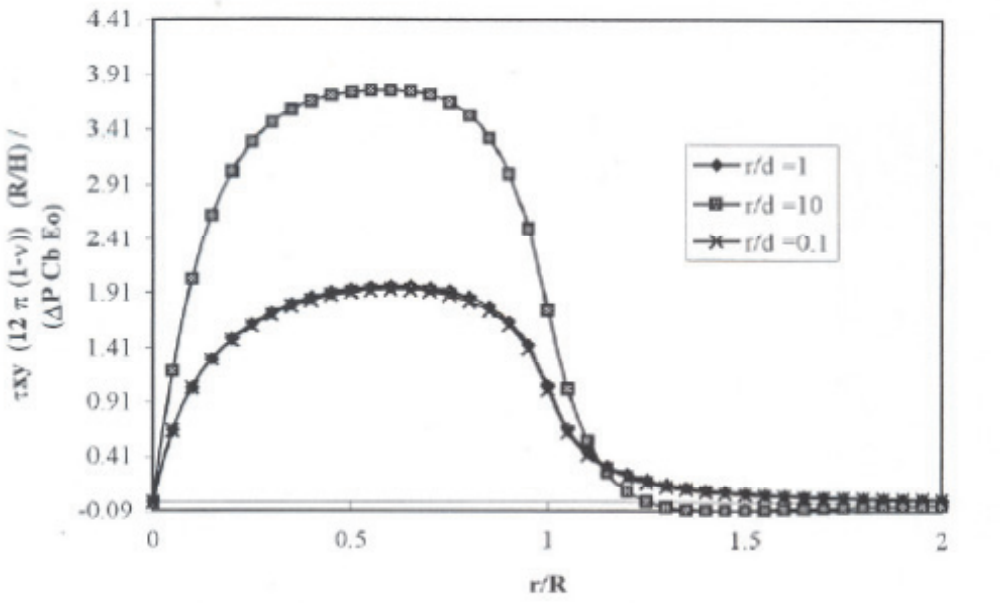

Fig.3. Normalized shear stress at the top of an axisymmetric reservoir with linear pressure change distribution

To illustrate the influence of pressure distribution shape on shear stress pattern and magnitude, we present in figure 4 the analytical solution for a sample reservoir of specific dimension (indicated in the figure) for both a uniform and linear pressure distribution. For both cases shear stresses are zero at the center of symmetry (center of the pressure change). In the case of uniform pressure, shear stresses reach a maximum near the reservoir flank.

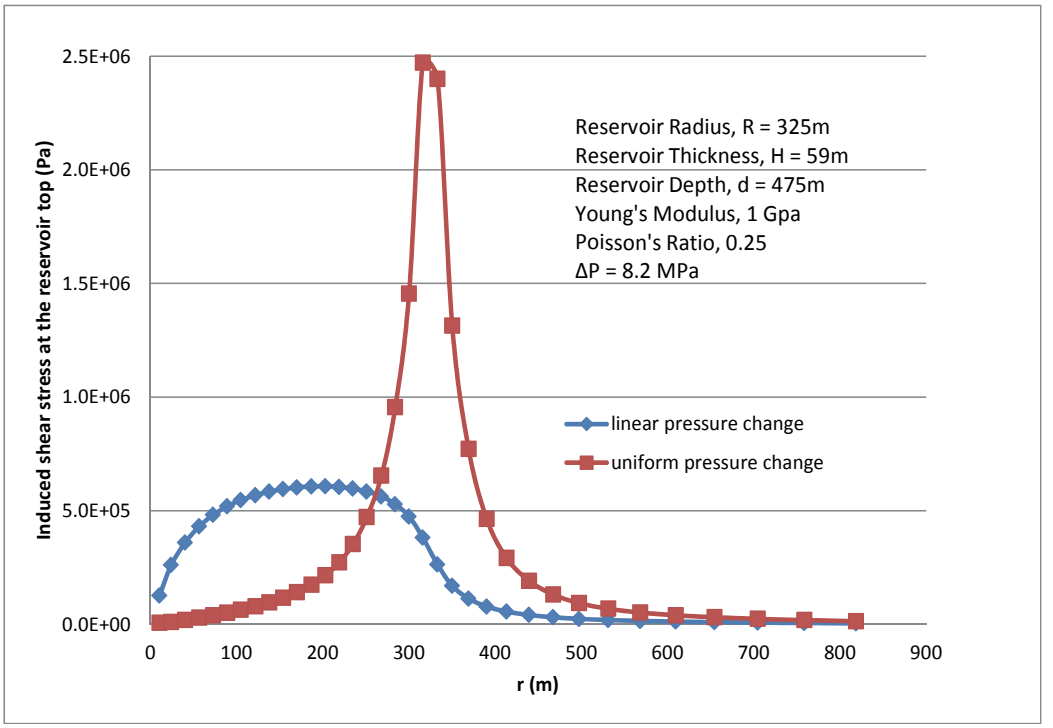

Fig.4. Comparison of induced shear stress with linear (blue) and uniform (red) pressure change for a sample axisymmetric reservoir

Although only a very few simple reservoir configurations can be solved analytically, the theoretical description nevertheless provides insight and guidance on relative risk factors. For example, it can be seen that induced shear stress magnitude increases with larger radius to depth ratio. But once a reservoir is deeper than about the distance of its radius, shear stress magnitude is relatively insensitive to depth and is instead controlled primarily by the ratio of reservoir thickness to reservoir radius. That is, pressure changes over a thicker reservoir interval will induce proportionately large shear stresses in the caprock than the same pressure change generated over a thinner reservoir interval. Analytical solutions can also be used for comparison and validation of numerical modelling approaches.

4. Integrated geology, transport flow, and geomechanical simulation to evaluate CO_2 injection effects

A general workflow developed and applied by GeoMechanics to evaluate injection (or production) effects, including induced stresses, possible fault activation or bedding plane slip, subsurface and surface deformation, and well damage risks, is presented in figure 5. The first step is to establish a 3D geologic model for the area, based on well log data, seismic data, and drilling data. The next step in the characterization process is to develop integrated fluid flow and geomechanical models to simulate CO_2 injection and migration, and to simulate the stresses and displacements induced by injection related pressure and temperature changes.

In summary, first a 3D static geologic model (or models) is established consistent with available seismic, log, and drilling data. Based on this 3D geometry and grid structure, fluid flow and geomechanical model are also established. In general the fluid flow models cover a smaller volume space than either the geology model or the geomechanical model, as the latter two must extend to the surface and beyond the lateral extent of the reservoir. For this particular project we use Rockworks for the static geologic models, TOUGH2 for the fluid and heat flow simulation, and FLAC3D for the geomechanical simulation.

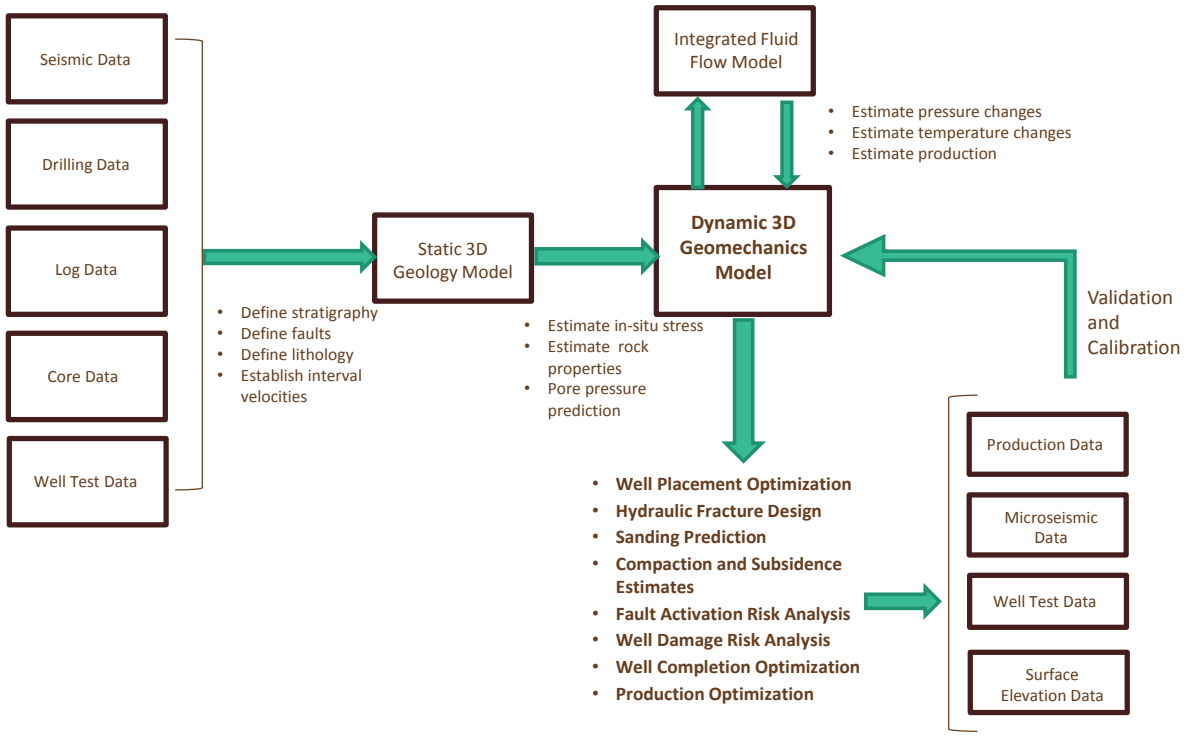

Fig.5. Generalized workflow for assembly and application of integrated geology, fluid flow, and geomechanical modeling

To illustrate the process and sample application, during the course of this project we created detailed geologic models for three large-scale geologic sequestration sites, encompassing a range of geologic settings. Modelling was completed for the Kevin Dome area in Montana, the Wilmington Graben area offshore Los Angeles, and Louden oil and gas field in Illinois. We present herein results for Kevin Dome, which is a relatively low risk operation, and for the Wilmington Graben, which is a relatively higher risk operation (as will be described later in this paper).

Initial static geologic models for each site was developed from stratigraphic and lithologic information collected from maps and wells located throughout the fields. The completed geologic models of each of these three sites were used as input for three-dimensional coupled transport flow and geomechanical models to investigate and describe caprock behavior, for a range of CO_2 injection conditions.

Pressure and temperature distributions were simulated using the TOUGH2 family of codes from Lawrence Berkeley National Labs. These have been developed to simulate multi-phase, multi-component fluid and heat flow in porous and fractured media. Pressure and temperature results from the TOUGH2 simulations were then used as input into three-dimensional geomechanical models to evaluate induced deformations and stresses within the reservoir and overlying caprock. The geomechanical simulation tool used was FLAC3D, with enhanced constitutive behavior functions developed by Geomechanics Technologies to model formation deformation, faulting, and bedding plane slip. To manage areas with uncertain geology, several geologic scenarios were simulated to determine the horizontal and vertical extent of the CO_2 plume after 30 years of injection. We developed and applied this combined and coupled fluid and temperature flow simulation and geomechanical simulation technique over a range of operating conditions (single and multiple injection wells at varying rates and temperature).

4.1. Kevin Dome, Montana

The Kevin Dome is located in Northern Montana. The area is being studied and characterized for large scale CO_2 sequestration by the Big Sky Carbon Sequestration Partnership (see www.bigskyco2.org for latest updates). The proposed sequestration site contains a low-sloping anticline structure composed of carbonate and detrital rocks. Studies are underway by the Big Sky Partnership to characterize injection into the Duperow formation, a zone of high porosity dolomite located at a depth of 1250 m (4100 ft).

For the GeoMechanics Technologies caprock integrity study, however, we were requested by US DOE to perform geomechanical analysis and risk analysis completely independent of the partnership efforts. We therefore collected and analyzed well log data and geologic data from Montana State public records in order to develop combined geologic, fluid flow, and geomechanical models for the area. Figure 6 presents a map view of the project area, with contours elevation of the Duperow Formation, and showing the areal extent of our geologic, fluid flow, and geomechanical model boundaries.

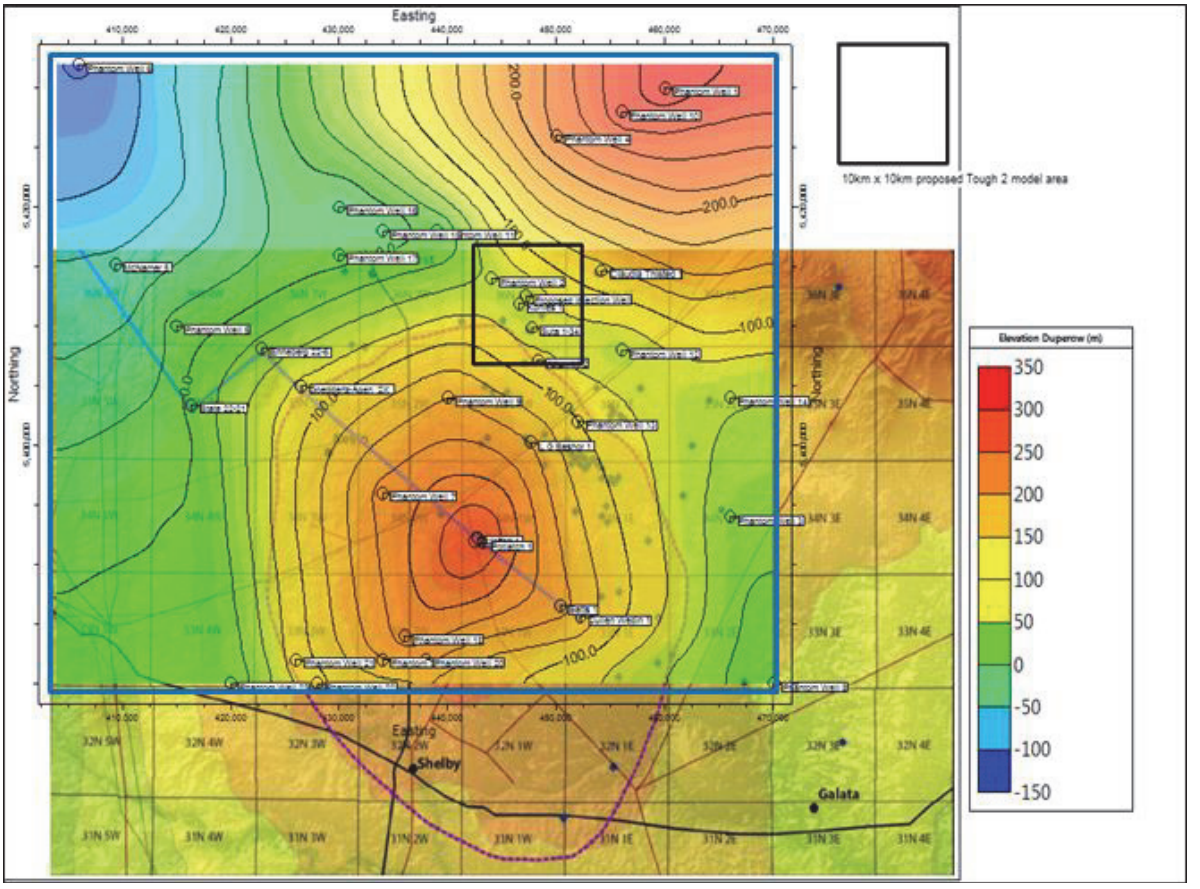

Fig.6. Kevin Dome map. Blue box marks perimeter of the geologic model domain. Black box indicates location of the 10km X 10km combined fluid flow and geomechanical model domains.

4.1.1. Geologic Information

First, a 3D stratigraphic and lithology model was constructed for the area (see Fig.7 below) based on well log marker data and available maps. This was constructed using RockWorks software. Well control is available but somewhat limited in this area (see available wells in white boxes of figure 6). While there is a great deal of hydrocarbon production in this region, it is generally limited to shallower formations. Only a few wells penetrate into the proposed, deeper injection formation. Fig.8 shows a cross section through the stratigraphic model centered on the proposed injection well. Digital sonic and density logs for wells State 22-21 and Potlatch O & R 1 were obtained and analyzed for rock mechanical properties.

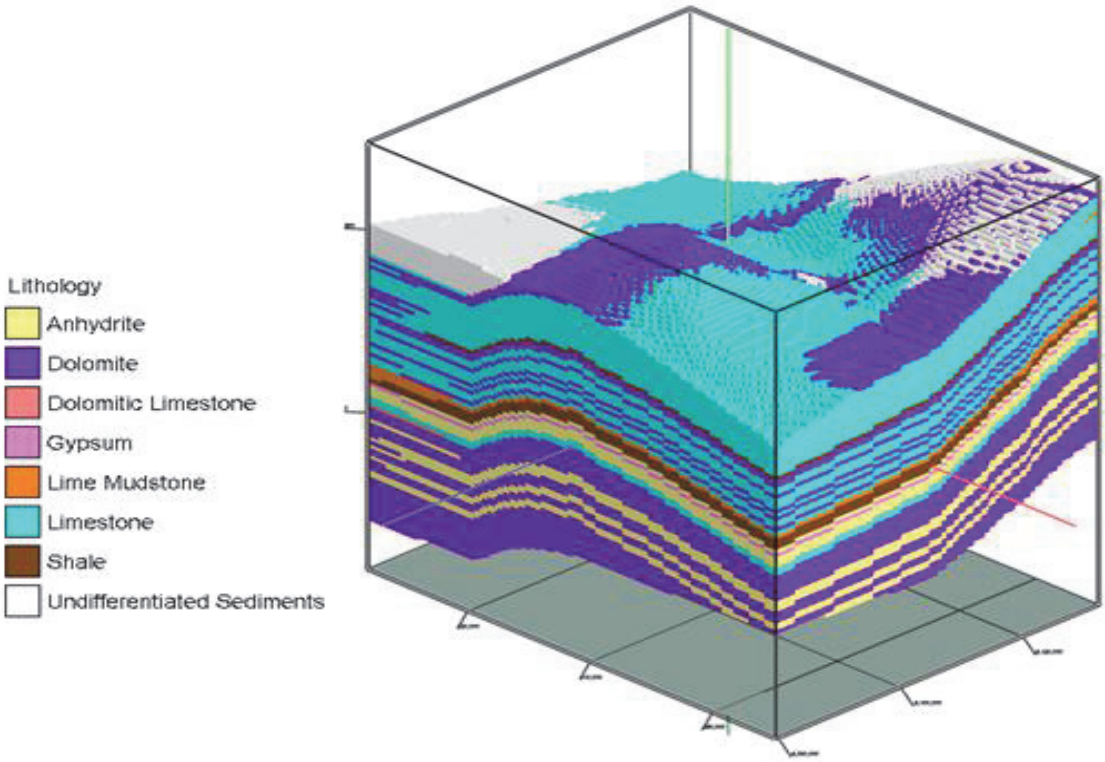

Fig.7. Lithology model developed by GeoMechanics for the Kevin Dome CO_2 injection analysis.

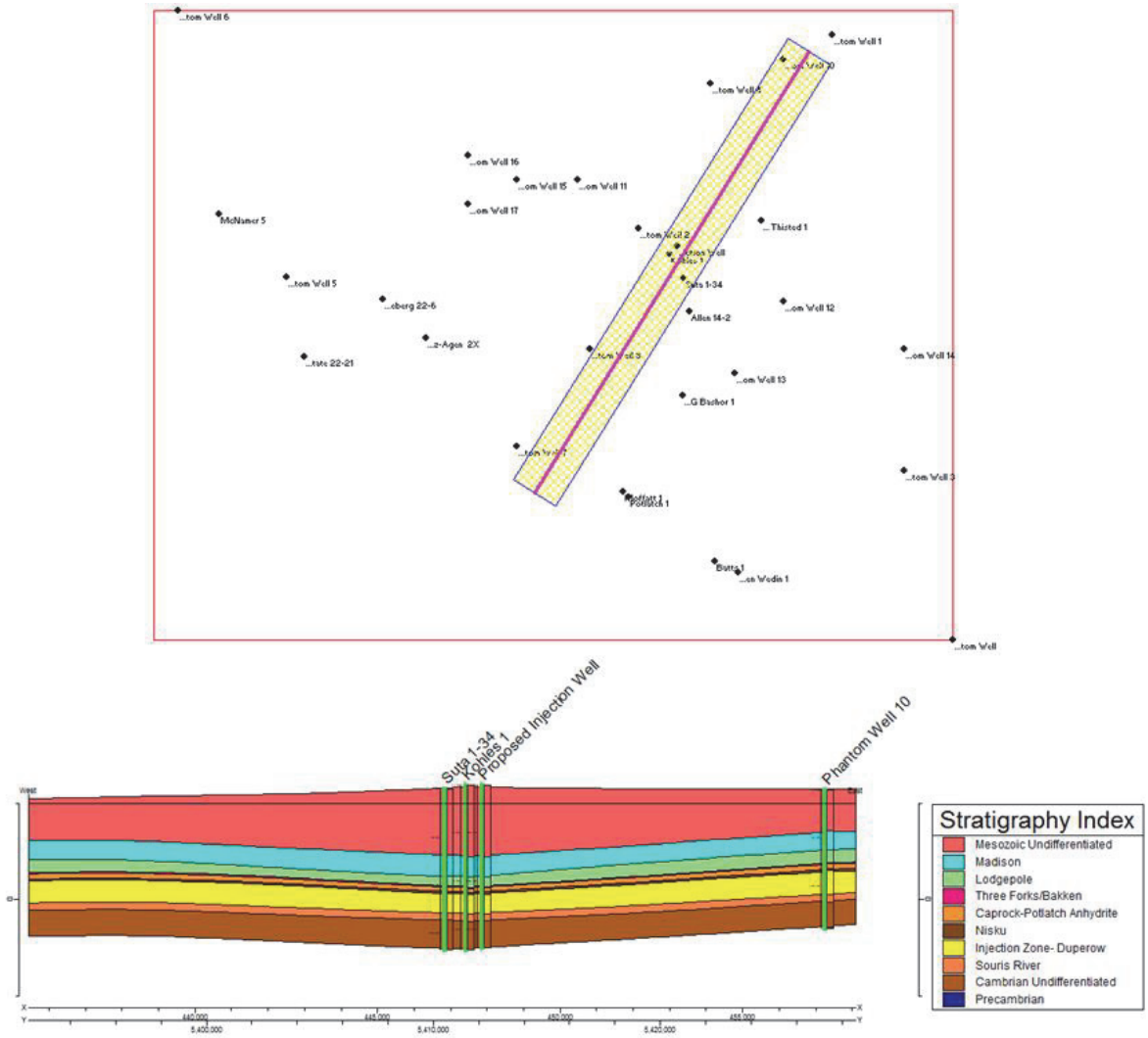

Fig.8. Cross section through stratigraphy model centered on proposed injection well.

4.1.2. Fluid Flow Migration Model

After establishing a 3D geology model, the next step in the process is to develop a 3D fluid flow model. For this step we developed a TOUGH2 fluid migration model using the PetraSim graphical user interface. The model established (see Fig.6 and Fig.9) is 10km X 10km in the lateral dimension and 1400m in the vertical direction, spanning a depth interval from -231.72 to 1174.8 m, and centered on the proposed injection well. The injection interval is between -75 m & -95 m (note: negative sign indicates below sea level), which is 1,250 m to 1,270 m below ground level. The mesh is finer around the well and in the injection interval; totaling 56,129 elements. The stratigraphy and lithology data from the RockWorks geologic model were input to the TOUGH2 model.

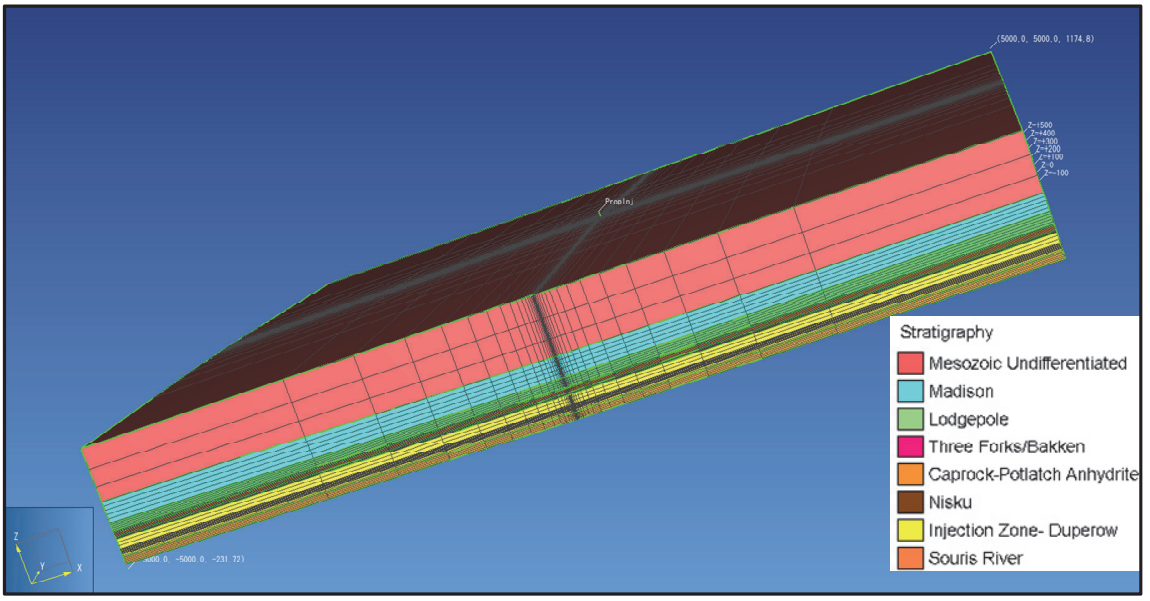

Fig.9. Fluid flow model mesh for Kevin Dome.

The density (kg/m^3), effective porosity (%), and three-dimensional permeability (mD) of each material were estimated from literature values. We gathered relative permeability and capillary pressure curves based on similar lithologies and in-situ conditions found near the Kevin Dome area. After we compared the formation depth, pore pressure, temperature, permeability and porosity properties typical for the Kevin Dome area, we chose the Muskeg Anhydrate, Wabamun Carbonate (low K and high K, respectively), and Calmar Shale as our reference formations for determining the relative permeability and capillary pressure curves by using Van Genuchten-Mualem function [18 & 19].

Initial temperature and pressure conditions were set consistent with well log data from this area. The surface temperature is set to 15.56 C (60 F), with 0.0145 C/m (0.8 F/100ft) temperature gradient. The surface pressure is set to 1.01325E5 Pa (14.7 psi), with 1.0857 Pa/m (0.48 psi/ft) pressure gradient. The side boundaries are set with constant pressure (initial gradient). We used the ECO2N module for supercritical CO_2 injection simulation, and simulated isothermal conditions for up to 50 years of constant injection pressure 1.62E7 Pa (2350 psi). This is about 17% higher than the initial pressure. About 15.4 million tons of CO_2 are injected over 50 years (0.308 million tons per year).

Fig.10 presents a top view of the resulting CO_2 plume migration after 50 years of injection. CO2 flow is well contained vertically beneath the caprock, and extends about 2000 m laterally away from the wellbore. **Error! Reference source not found.** shows the pressure contour in NE-SW and NW-SE directions, centered on the injection well, at the end of 50 years injection. Fig.12 shows the pressure profiles at $\text{time} = 0$ and $\text{time} = 50$ years on a horizontal section through the injection zone, centered at the injection wellbore. The pressure increase at the injection well is about 2.5 MPa (360 psi). This pressure change profile is subsequently used as input to the geomechanical model, in order to estimate induced stresses and deformations.

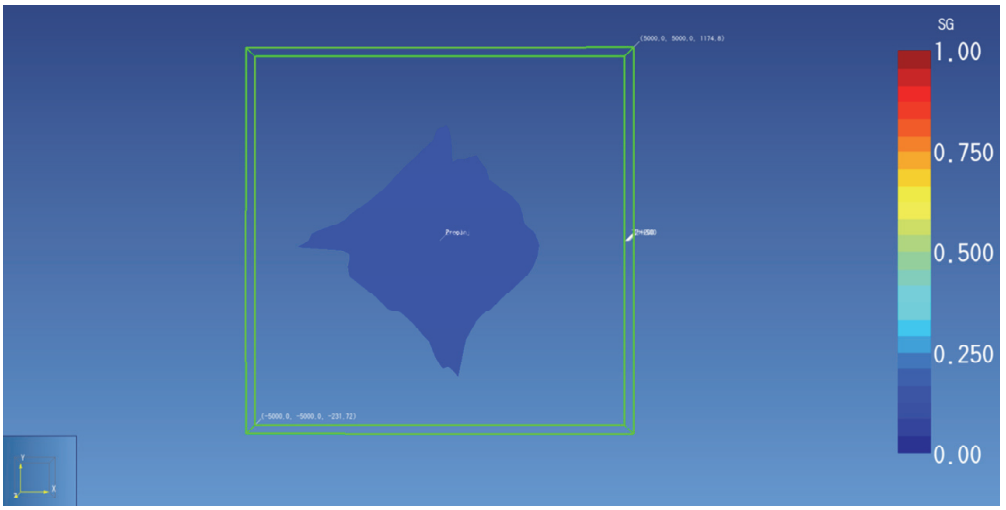

Fig.10. CO_2 supercritical gas plume after 50 years of injection – top view.

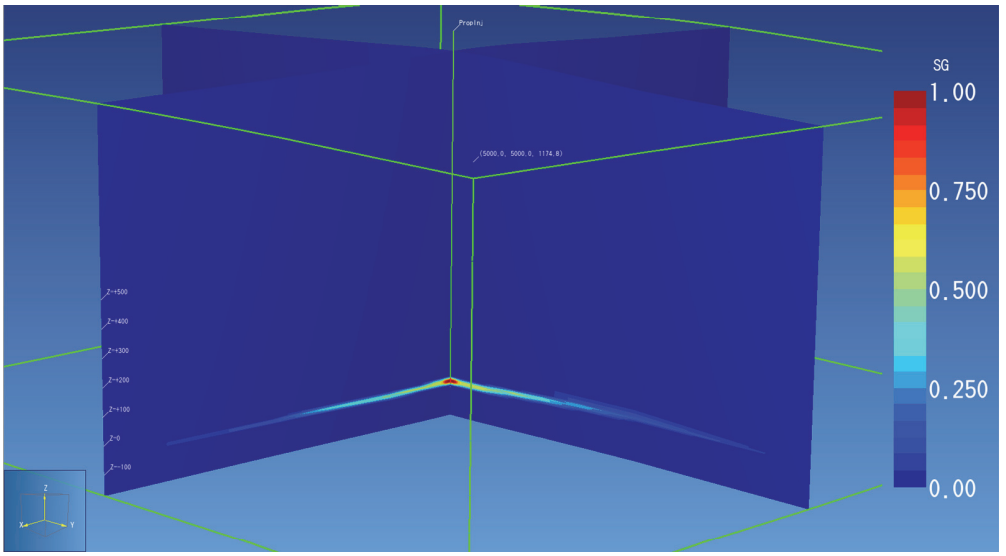

Fig.11. Supercritical CO_2 saturation contour centered on injection well, in NE-SW and NW-SE directions.

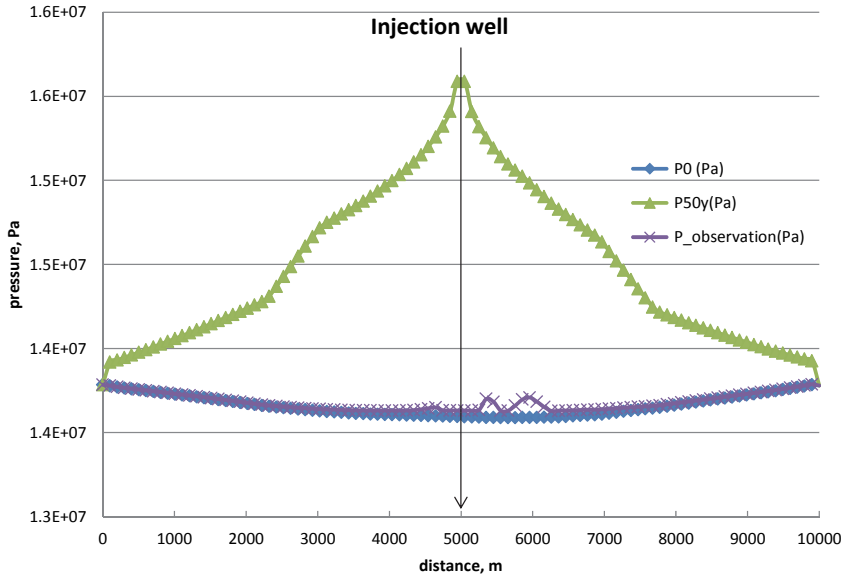

Fig.12. Pressure profile in the injection zone, centered on the injection well, in NE-SW direction.

4.1.3. Geomechanical Model for Kevin Dome

We next developed a 3D geomechanical model for Kevin Dome, mapping grid information and data from the geology and fluid flow models. The dimensions of the geomechanics model are 10,000m x 10,000m in the lateral direction, and about 2500 m in the vertical direction, extending from the surface about 1175m above sea level to 1345 m below sea level, and centered on the injection wellbore. The model has a total of 144,000 elements, with a finer mesh near the injection well and in the Duperow injection formation (Fig.13).

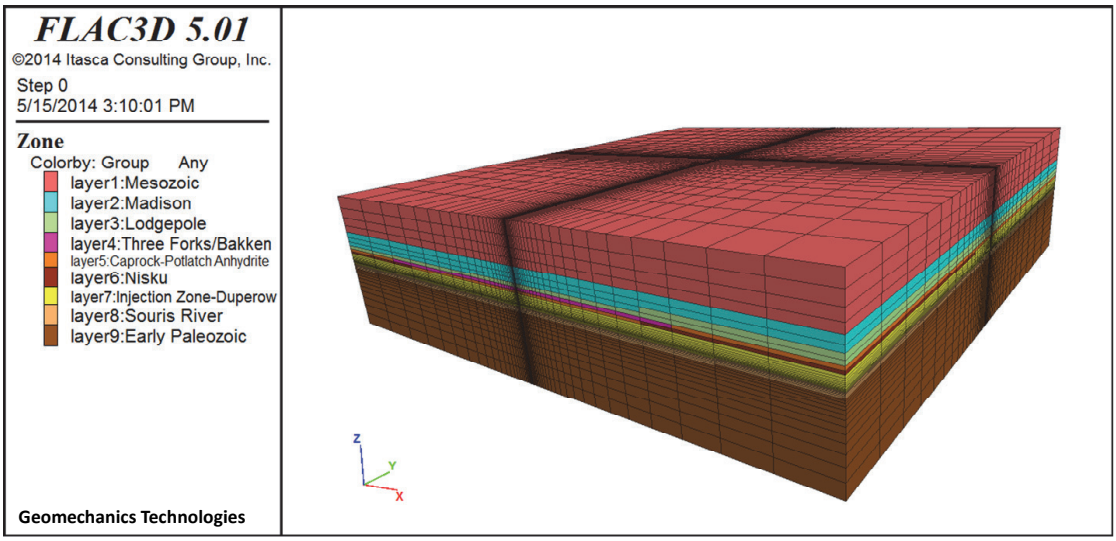

Fig.13. 3D geomechanics model established for Kevin Dome

The mechanical properties of each formation were estimated from log data, as no laboratory core test data are available. We applied roller boundary conditions on all surfaces except the top surface, which is free to move in both vertical and lateral directions. We then simulated the induced stress and displacement during 50 years of injection, by applying pressure changes from the fluid flow simulation to the geomechanics model. The resulting surface deformations are presented in Fig.14. The maximum displacement is above the injection well, with a maximum uplift of about 5 mm. This is relatively minor, primarily due to the low pressure increase and relatively stiff material properties.

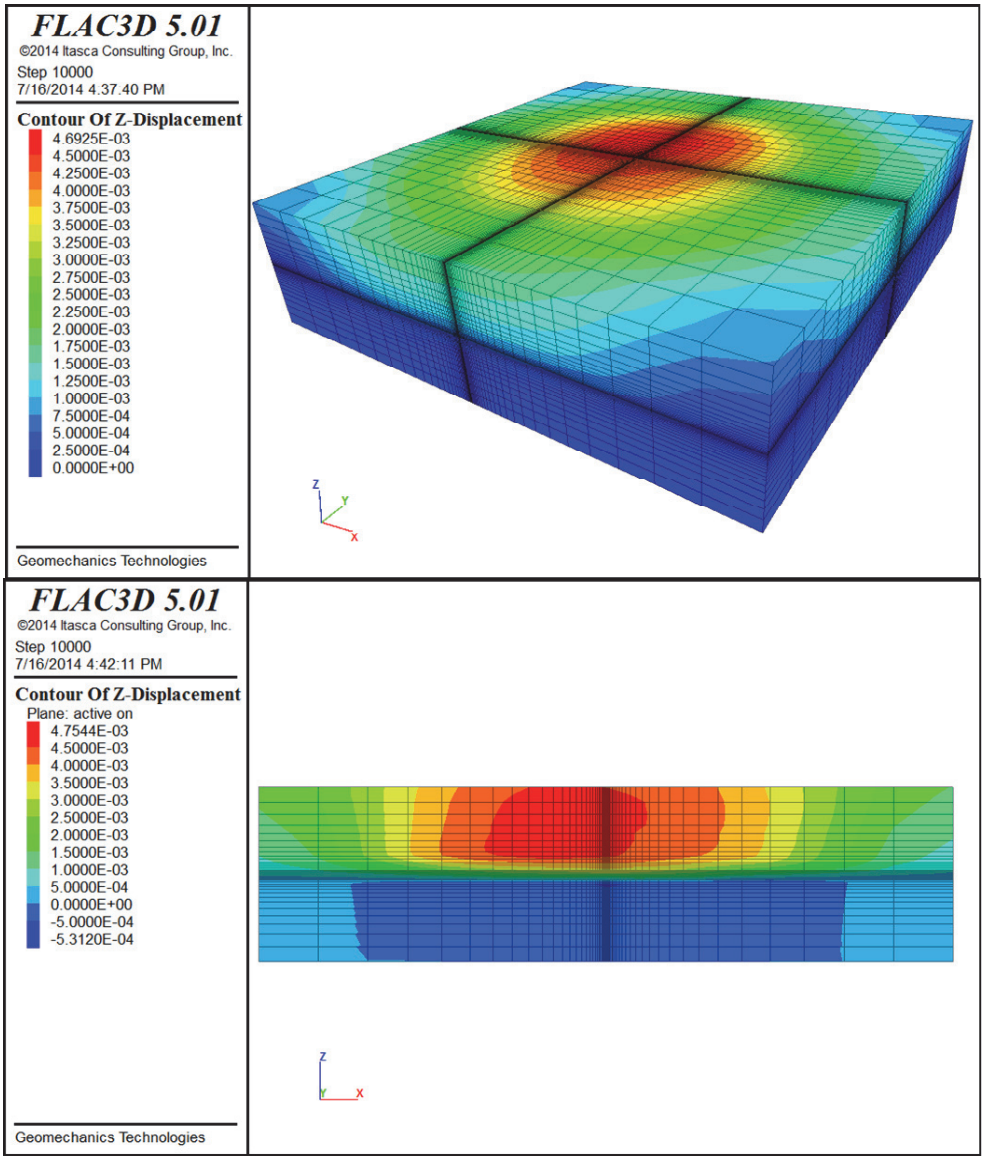

Fig.14. Vertical displacement: 3D view (top) and cross section (below), after 50 years of injection (meters).

We present in Fig.15 cross section views of the induced horizontal stresses. Compressive stresses are induced within the injection interval (zone of increased pressure), while tensile stresses are induced above and below the

injection zone. The maximum induced horizontal compressive stress is about 1.4 MPa (about 200 psi). The stress changes induced by injection operations in this case are relatively small compared to in-situ stresses and compared to estimated shear strength properties for the matrix material and bedding planes. Given these low values, there is no significant risk for caprock fracturing or fault activation.

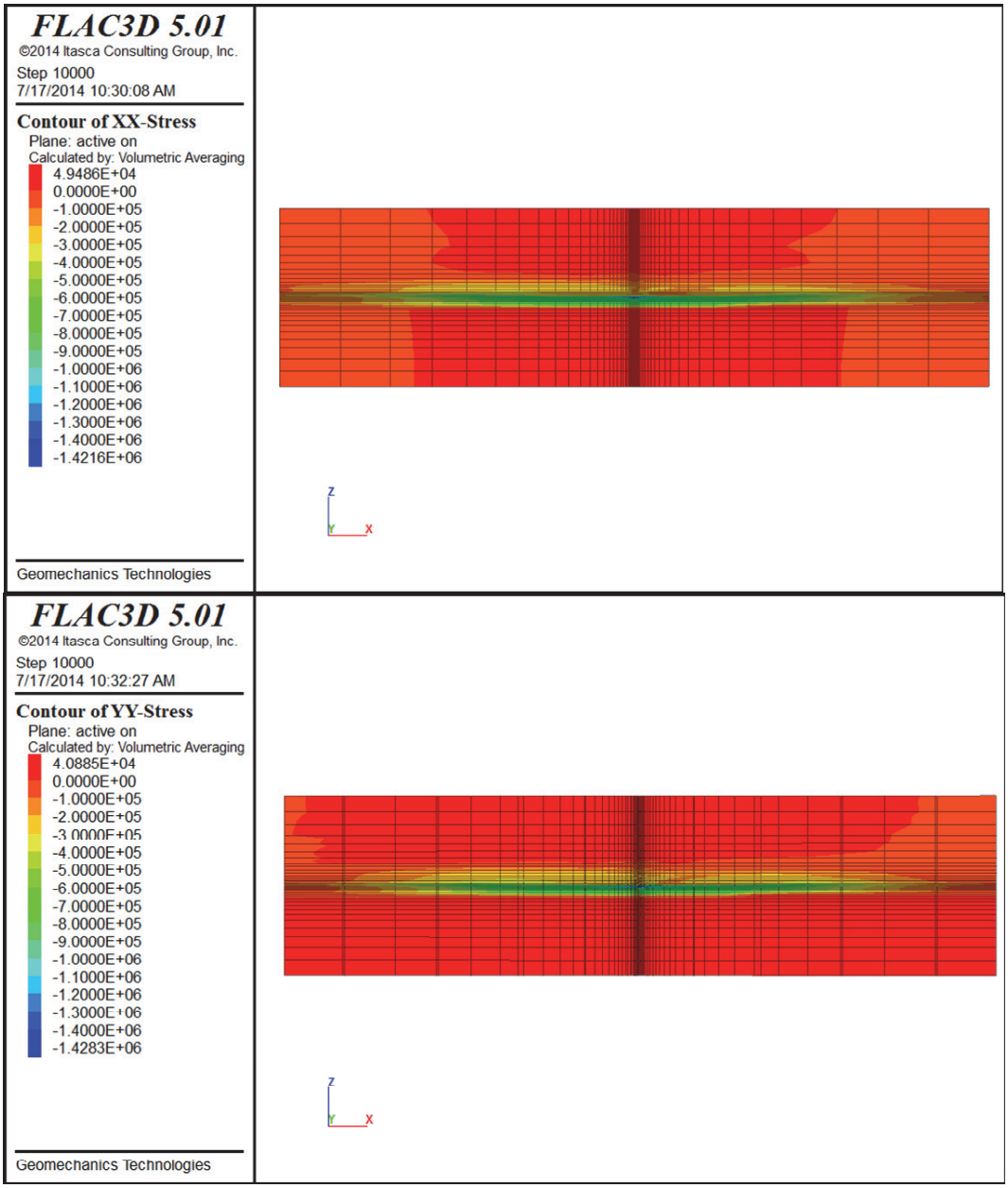

Fig.15. Plot contours of induced horizontal stresses after 50 years of injection, including E-W (top) and N-S (lower) normal stress, in Pa.

Fig.16 the induced horizontal shear stresses on N-S and E-W sections. These are quite low, with maximum magnitude only on the order of 3.0E+4 Pa.

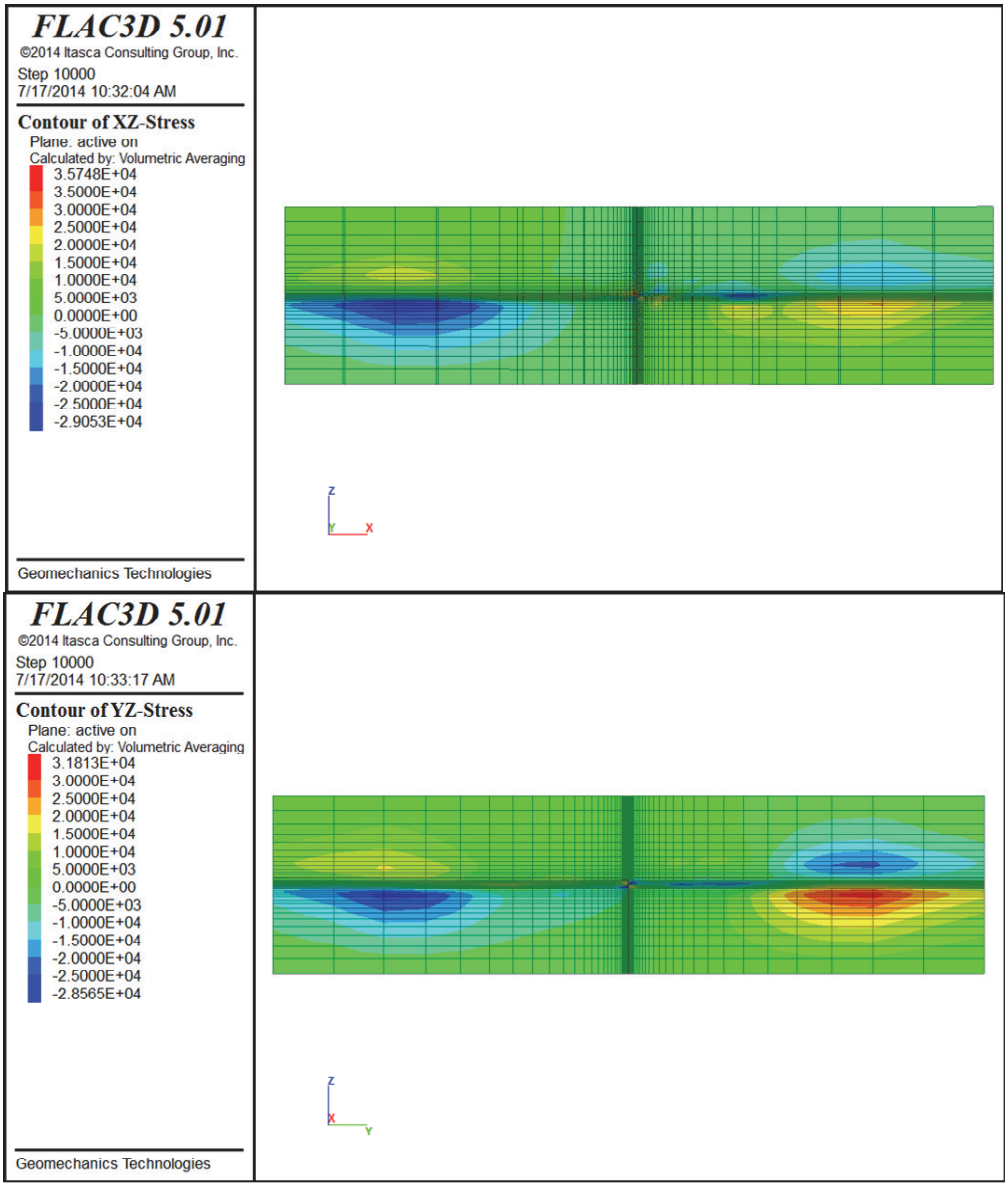

Fig.16. Plot contours of induced horizontal shear stresses after 50 years of injection, displayed on E-W (top) and N-S (lower) sections, in Pa

4.2. Wilmington Graben, Offshore Los Angeles, California

The Wilmington Graben is located offshore Los Angeles, California (Figure 17 below). The area is being studied and characterized for large scale CO_2 sequestration by GeoMechanics Technologies under DOE contract FE0001922. That effort is more fully described in a companion paper "Characterization of Pliocene and Miocene formations in the Wilmington Graben, Offshore Los Angeles, for large scale geologic storage of CO_2" (see also www.socalcarb.org). The graben is situated between the Palos Verdes fault to the west and the Thums-Huntington Beach fault to the east. The geologic setting is characterized by turbidite deposits composed of graded sequences of sand, silt, and shale.

Pliocene and Miocene sediments in the Los Angeles Basin are massive interbedded sand and shale sequences known to provide excellent and secure traps for oil and gas. The area contains several billion-barrel oil and gas fields, including the giant Wilmington Field in Long Beach (more than two billion barrels produced to date). These formations have been used by Southern California Gas Company for large-scale underground storage of natural gas at half a dozen locations throughout the Los Angeles basin for more than fifty years, demonstrating both the storage potential and security of these formations for CO_2 sequestration.

Fig.17. Wilmington Graben location, power plants, and refineries within the Los Angeles geologic basin.

4.2.1. Geologic model

The initial geologic characterization effort included assembly and analysis of log data from a dozen existing wells located within both State and Federal waters, and combination of this information into a common database. Several key geologic horizons markers were identified at each well location. Lithology versus depth was also identified for each well, separated into four categories for sand, shale, sand-shale interbed, and silt.

To further characterize the area and extend the geologic horizon beyond the discrete well locations in 3D, 3D seismic data available for a portion of the Wilmington Graben was re-processed and analyzed. An additional 175km of 2D marine seismic data was collected in a "data gap" area, using ship borne seismic arrays provided by Cal State Long Beach.

Finally, two new wells were drilled by GeoMechanics Technologies in the north Graben area to establish additional formation characterization data in both the Pliocene and Miocene intervals. Core samples were taken in each well, and measurements made of porosity, permeability, and rock mechanical properties.

Given the key stratigraphic horizons established from seismic data, and lithology versus depth determined from log data, inter-well interpolation was applied to create both stratigrahic and lithology models for the entire 3D volume comprising the Wilmington Graben. The 3D lithology model and an associated fence diagram is provided in figures

The offshore Wilmington Graben lies within a turbidite depositional environment. Lithology is known to vary both vertically and laterally. A simple interpolation between wells can sometimes create an overly simplified lithologic model. Seismic horizon data can inform the geologist of general stratigraphic trends, but can not completely resolve the uncertainty in lateral variation of lithology. To account for such variation and uncertainty, therefore, we considered multiple geologic interpretations of the available data with varying ratios of sand and shale. We developed and considered several alternative lithology distributions, each of which honor the general stratigraphic trend and the specific lithology distribution at each well. These include a baseline geologic model, a high shale geologic model, and low shale geologic model, each of which were considered in subsequent fluid flow simulations.

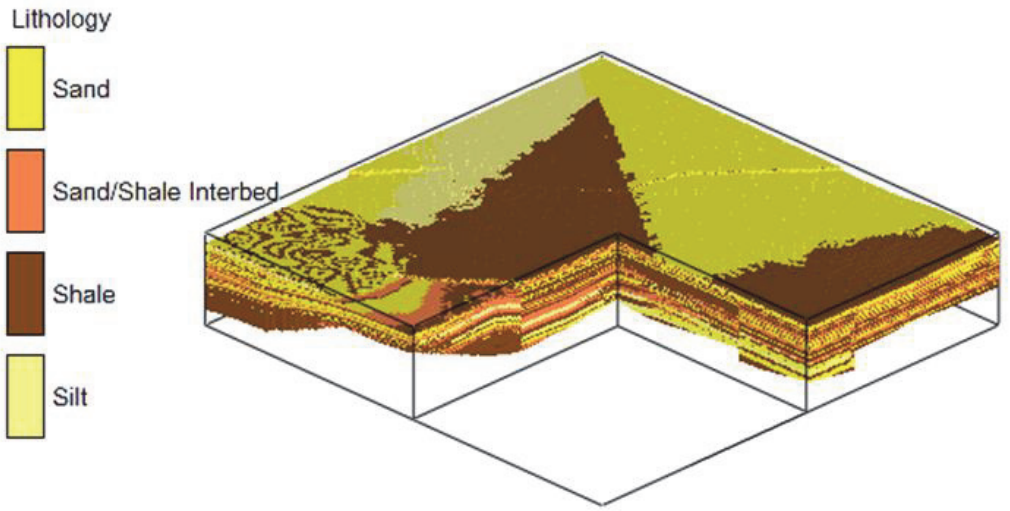

Fig.18: 3D lithology model with cut-away view.

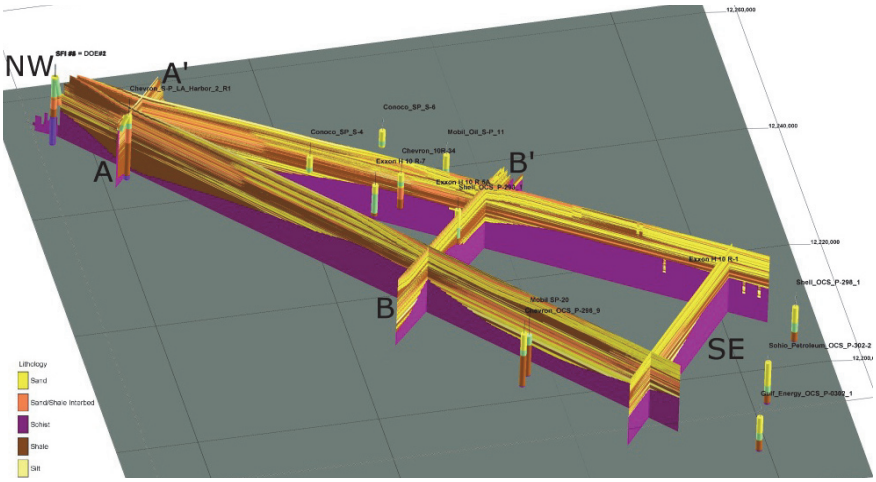

Fig.19. Geologic fence diagram for the Wilmington Graben with lithology interpolated between known wells.

4.2.2. Fluid flow model for the Wilmington Graben

Two areas in the middle and in the northwest of the graben were chosen for fluid flow and geomechanical modelling, as indicated in Figure 20. We present herein results for the middle graben area.

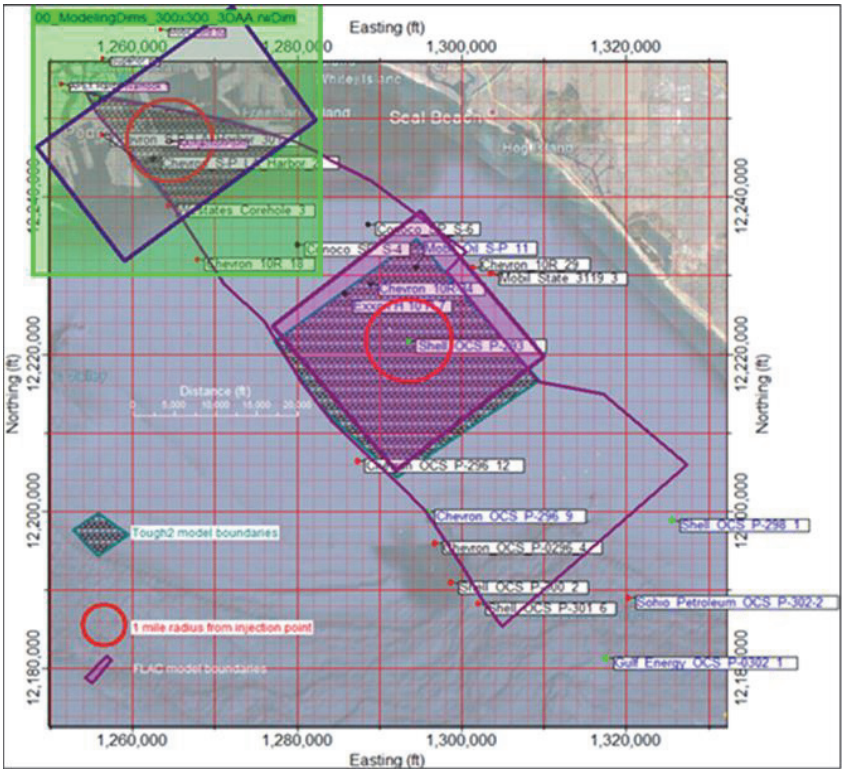

Fig.20. Integrated fluid flow models (shown in hatched area) and geomechanical models (shown in purple overlays).

The conceptual fluid flow model was created by mapping the geology from the RockWorks model into a TOUGH2 flow model (Fig. 21). The full conceptual model is shown in Fig. 22. As the model is bounded on the SW and NE by the Palos Verdes and Thums Huntington Beach faults, respectively (which are known to be sealing), these boundaries were set with no-flow conditions. The NW and SE boundaries of the model were defined as constant pressure conditions (depth dependent).

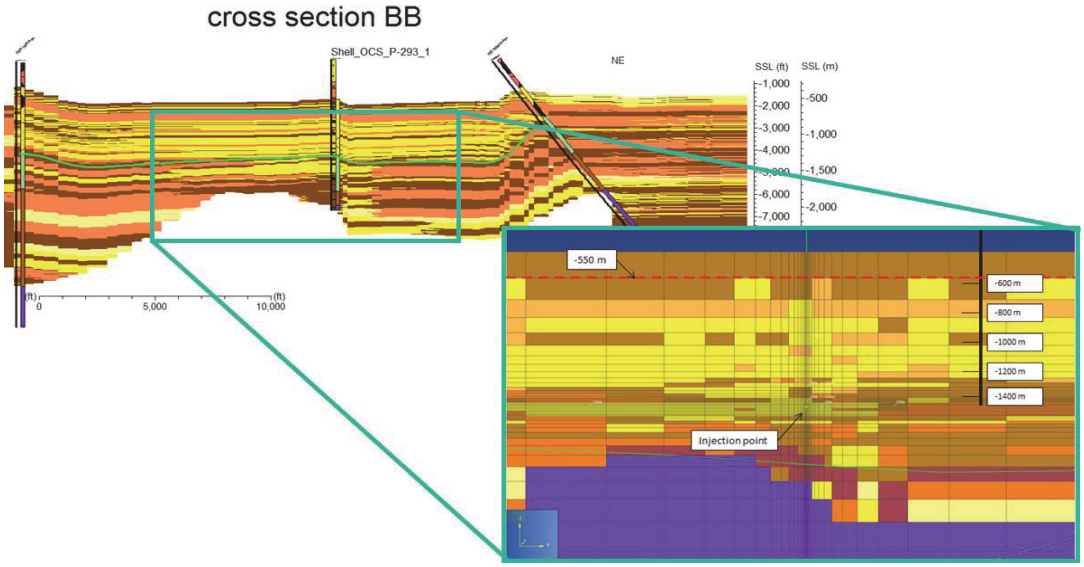

Fig. 21. Mapping of lithology from RockWorks model to TOUGH2 model.

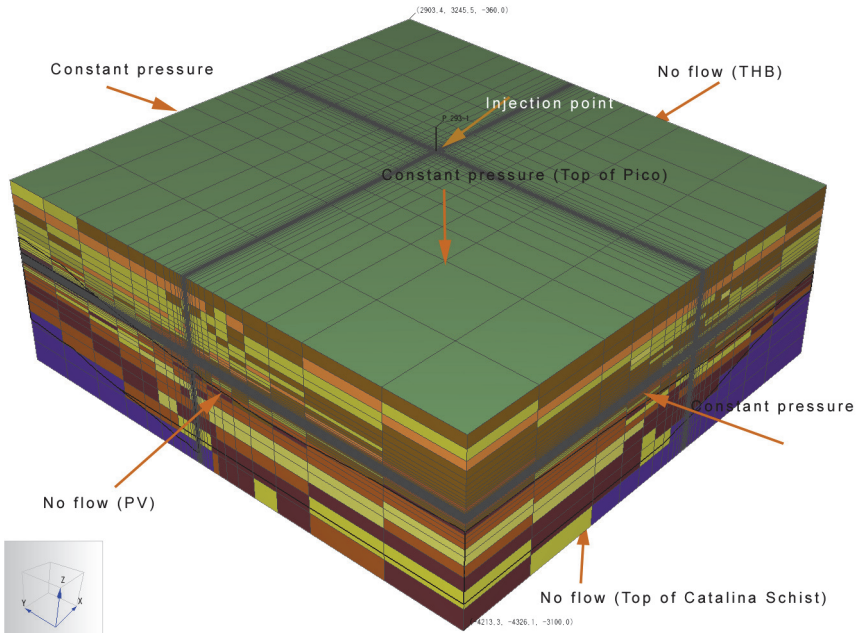

Fig. 22. 3D flow model for mid graben area.

We simulated thirty years of injection at about 1 million metric tons per year into a sand interval approximately 50m thick. The injection was followed by fifty years of monitoring. The simulation results for the geologic baseline model indicate that after 30 years of injection, the CO_2 plume migrated and extended to a distance of about 1,000m (3,280ft) in the horizontal direction and 450m (1,500ft) in the vertical direction, indicated in figures 23 and 24.

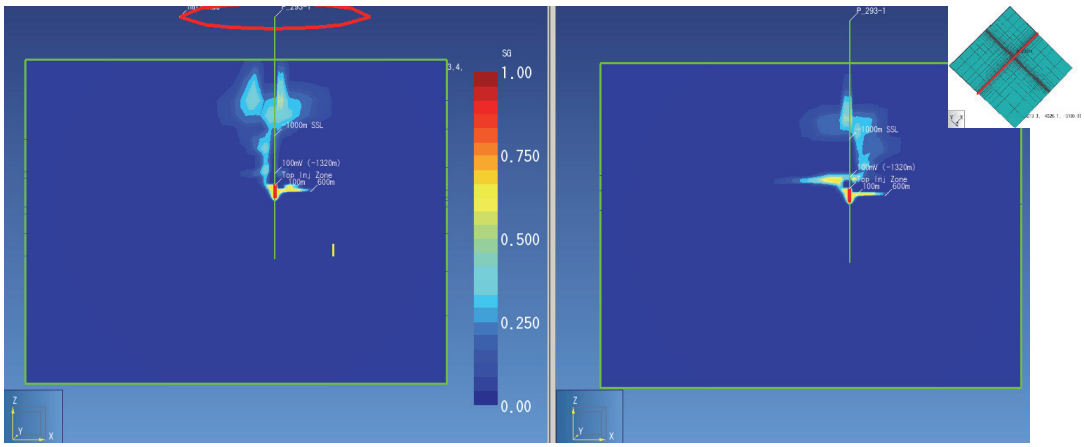

Fig. 23. CO2 migration in baseline model (left) and high shale model (right), both after 30 years of injection; SW-NE cross sections.

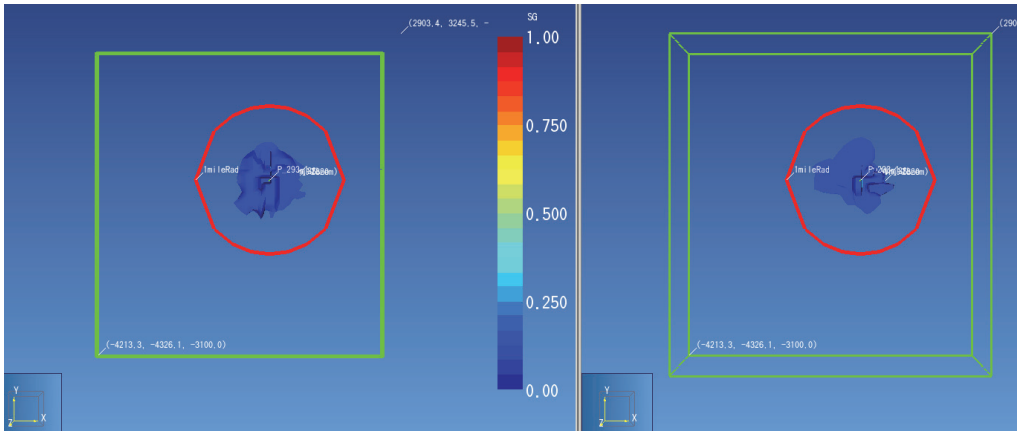

Fig. 24. CO2 migration in baseline model (left) and high shale model (right); both after 30 years of injection; top view.

4.2.3. Geomechanical model for the Wilmington Graben

A geomechanical model was also assembled for the central graben area. The purpose was to assess stress changes induced by injection operations, fracturing risks, fault activation risks, and surface deformations. Figures 25 and 26 present illustrations of the geomechanical model for the central graben area. The dimensions of this model are about 8500 m in the lateral directions and 2950 m in the vertical direction, extending below the injection interval to the seafloor. We apply roller boundary conditions on all surfaces except the top surface, which is free to move in both vertical and lateral directions.

Mechanical properties for varying layers were determined with sonic logs, calibrated with triaxial rock mechanics testing on core samples. The Palos Verdes and THUMS Huntington Beach faults serve as the no-flow side boundaries of the model, consistent with the fluid flow model. The model is initiated with gravitational loading and initial stresses determined from step-rate testing and borehole breakout analysis. Initial pressure and temperature as a function of depth were also determined for the area. The loading of the model is input via the change in pressure and temperature determined from the fluid flow simulation (i.e. a one-way coupling process). Note that to first approximation, material dilation or compression is related to the change in pressure times compressibility and to the change in temperature times thermal expansion. Increased pressure acts to expand the formation rock, while decreased temperature act to contract the rock. The surrounding materials resist this expansion and/or contraction, resulting in stresses being induced both within the interval experiencing pressure and temperature change and within the surrounding formation material.

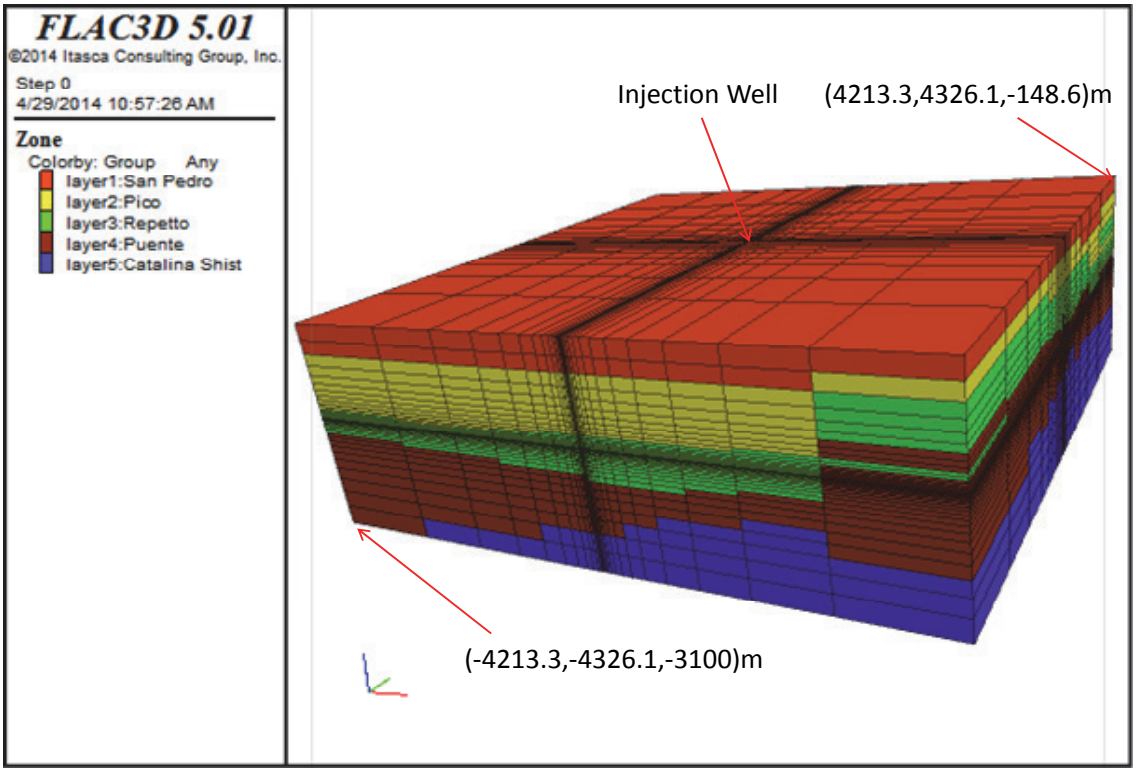

Fig. 25. 3D geomechanical model for the central Wilmington area.

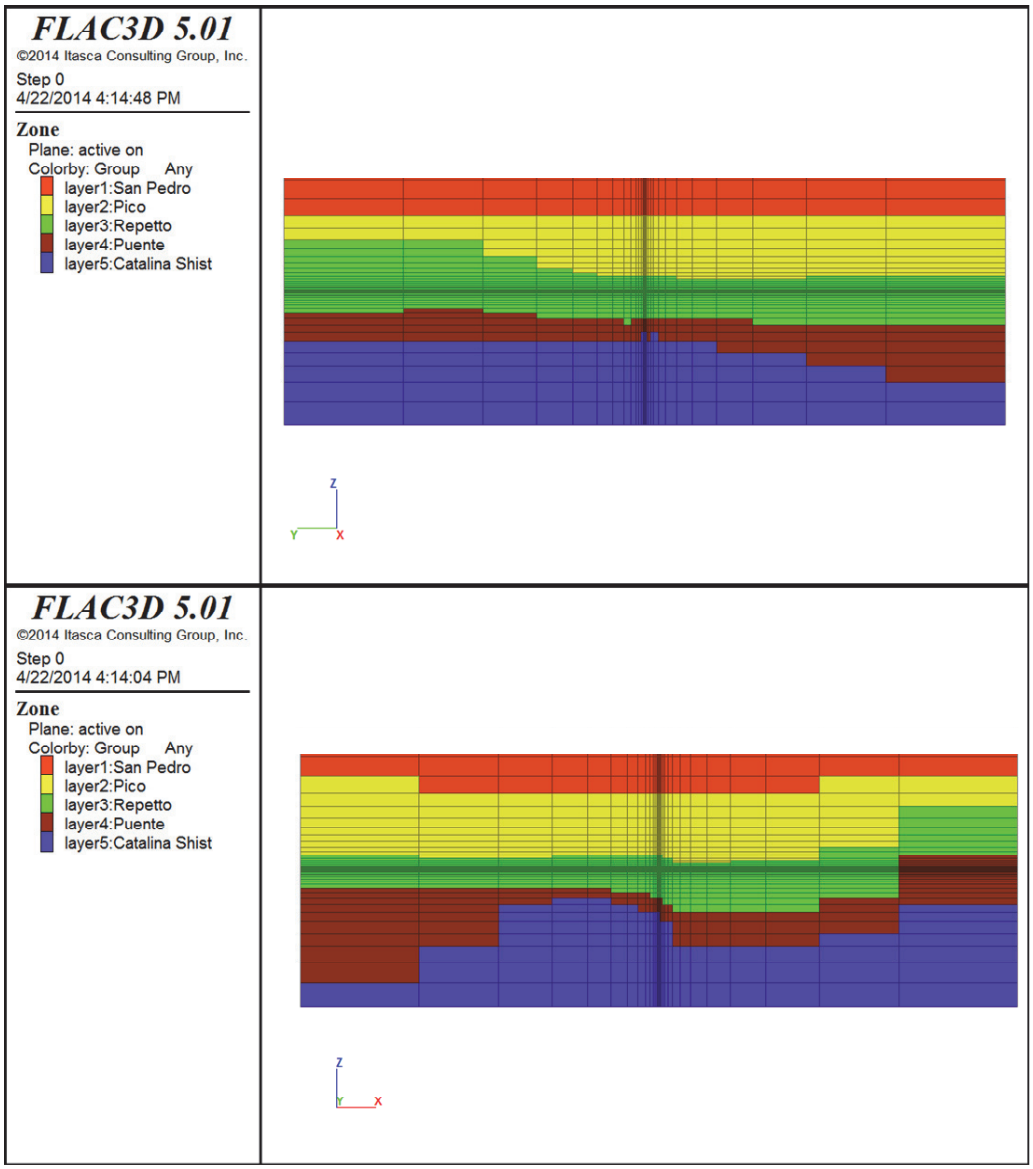

Fig. 26. Geomechanics model cross sections centered on the proposed injection wellbore; NW-SE (top) and NE-SW(bottom) directions.

Figure 27 presents the change in pressure determined from the fluid flow model and applied as loading to the geomechanical model. Pressure changes are relatively minor, generally less than 1 MPa throughout the region of CO_2 migration. Figure 28 illustrates the horizontal stresses induced by such pressure change. Compressive stresses are induced within the pressurized areas and tensile stresses are induced above and below. These induced tensile stresses, however, are significantly below in-situ compressive stresses for the area, so that risks for caprock fracturing are very low.

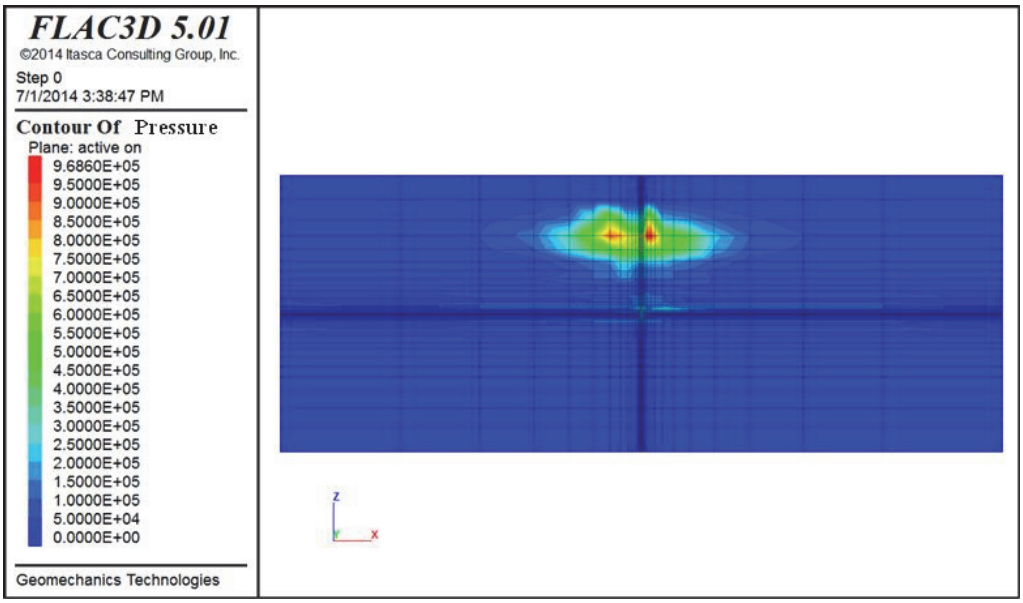

Fig. 27. Pressure change determined from fluid flow model and input into geomechanical model (Pa)

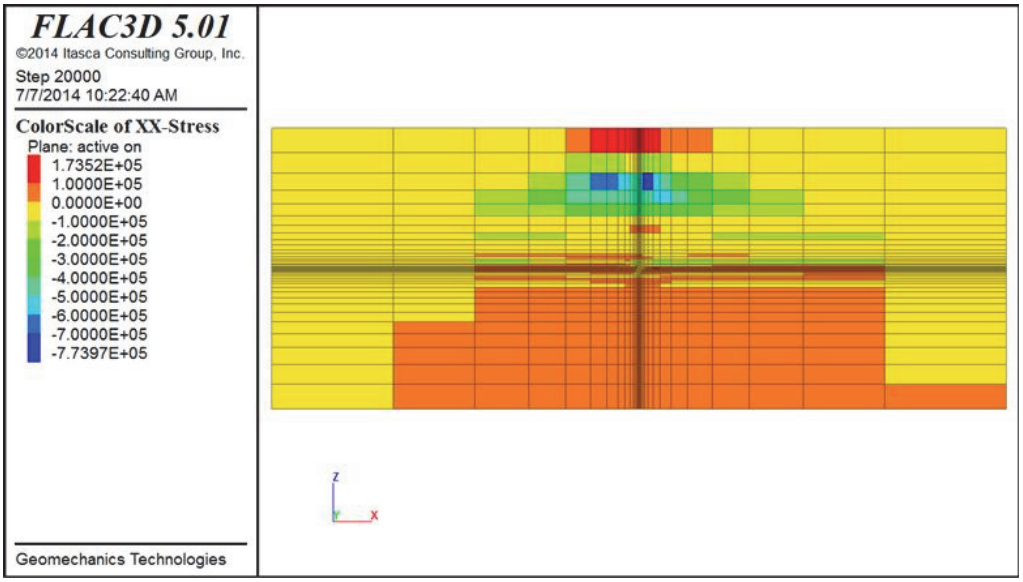

Fig. 28. Resulting induced horizontal stress change (Pa)

5. Development and application of a quantitative risk and decision analysis tool to assess caprock integrity

We next describe a Quantitative Risk & Decision Analysis Tool (QRDAT) developed for caprock integrity evaluation, with the aim of assessing the potential for leakage during CO_2 injection. For this purpose we have established a set of parameters (risk factors) that influence the likelihood of caprock failure. We established order of magnitude value ranges for each parameter, which, when applied to particular geologic and operational settings, enable quantification of risk and offer a means by which to compare potential and active storage sites.

We consider three primary leakage mechanisms. These are tensile fracturing of the caprock, fault activation, and well damage. The set of risk factors can be divided into three main groups:

1. Mechanical state of the storage system, which includes stresses, pressures and faults;
2. Caprock and storage zone system, including reservoir and caprock geometry and properties; and
3. Operations, which include the status of the wells and injection practices.

5.1. Mechanical State Factors

5.1.1. Desired maximum formation pressure/effective minimum horizontal stress

The higher this ratio, the higher the risk for caprock failure. This number is a measure on how close the pressure in the formation is to the failure pressure, as fracturing occurs when the minimum horizontal stress is exceeded by the pressure in the reservoir.

5.1.2. Desired maximum formation pressure/discovery pressure

This ratio is a measure of the pressure increase in the reservoir. The higher this ratio, the larger the pressure increase in the caprock-storage zone system. The magnitude of pressure increase controls the potential for tensile and shear failure in the caprock and so poses risks for CO_2 containment.

5.1.3. Maximum formation pressure/formation depth

Higher formation pressure increases the risk for caprock failure. This value, however, needs be normalized to the formation depth to take into account the fact that high pressures are less influential with increasing depth due to countervailing pressure increases from increasing overburden load. The higher this ratio, the higher the risk for integrity loss.

5.1.4. Stress regime

Simple stabilization relations imply that a compressional stress regime will have the highest risk for reactivation during CO_2 injection, as CO_2 pressure increase will have a destabilizing effect on thrust faults, whereas it has stabilizing effect on normal faults (Fig 29). This only refers to the normal stresses induced by pressure increase. It does not refer to possible direct migration of fluid into the fault zone, which can destabilize either type of fault by reducing the normal effective stress acting to keep the fault from slipping.

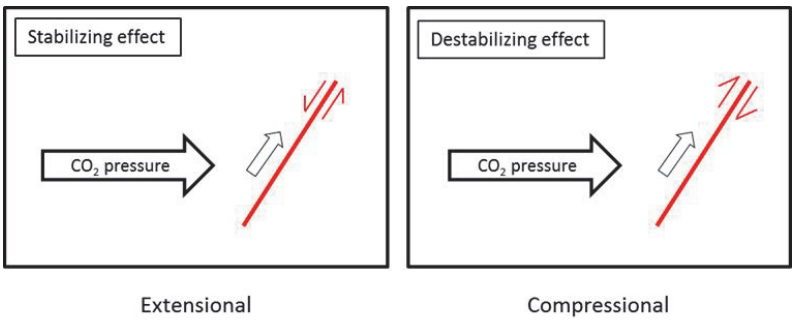

Fig 29. Induced horizontal stresses due to injection tend to stabilize normal faults and destabilize reverse faults

5.1.5. Stress ratio

The stress ratio is defined as σ_3/σ_1. Modelling studies for extensional stress regimes have shown that lower stress ratios lead to larger absolute fault slip magnitudes [22& 23]. In general, stress ratios are on the order of 0.5-0.7. Lower stress ratios lead to greater fault reactivation risks due to enhanced arching of the resulting normal stress. This causes a larger normal than shear stress ratio and so a greater chance of fault activation.

5.1.6. Fault boundaries

Faults can be activated by supercritical CO_2 encroachment. Stable faults are in equilibrium with the stresses acting on the fault plane. An increase in fluid pressure due to pressurized CO_2 entering the fault plane decreases the effective normal stress on this fault plane. When the fault plane approaches critical stress needed to initiate fault movement, this pore pressure increase may activate the fault. There is consensus that faults may act as flow paths, at least shortly post-failure [24]. The presence of one or more close faults that extend far into the caprock increases the risk of caprock integrity loss. Additionally, Orlic et al. [25] have demonstrated that stress concentrates on fault planes at interfaces between different lithologies, as exist between reservoirs and caprocks. Therefore, fault reactivation may be more likely at the caprock-reservoir interface, increasing this location's sensitivity to integrity loss.

5.1.7. Natural seismicity

High natural seismicity clearly poses a risk for caprock integrity loss. In regions with strong natural seismicity, the presence of pre-existing faults and fracture networks can be expected, which offer potential conduits for fluid migration, and generally reduce caprock integrity.

5.2. Caprock-Storage Zone System Factors

5.2.1. Storage zone lateral extent/depth and caprock lateral extent/thickness

These parameters assess the lateral continuity of both the reservoir and caprock by normalizing it to a fixed value (formation depth and caprock thickness, respectively). Clearly, the more extensive a formation is in the lateral direction, the smaller the chance that CO_2 will reach a spill point and migrate upwards. Therefore, high ratio values for these parameters indicate low failure likelihood.

5.2.2. Storage zone thickness/ depth

High values for this ratio correspond to a relatively thick reservoir at relatively shallow depth, indicating relatively large volumes of CO_2 stored relatively close to the surface. This combination has a major implication if failure in the caprock occurs:the release of a large amount of CO_2 without far to migrate upwards to reach the surface. Thus high ratio values here correspond to high risk.

5.2.3. Caprock strength

A stronger caprock has a lower risk for caprock integrity loss, due to a lower risk for both tensile fracturing and the onset of new faults in the caprock. A fracture develops only when the compressive strength in a rock is overcome, so the higher the unconfined compressive strength the lower the risk for the development of fracture networks. Note that a stronger caprock may lead to higher pressure build-up, which may lead to overburden and surface heave (e.g., In Salah [26]). Bending of the caprock during uplift may lead to the development of shear stresses at the top of the caprock [27], but no cases of caprock failure due to surface heave have been reported thus far.

5.2.4. Caprock permeability

Relatively permeable caprocks may lead to loss of CO_2 containment, simply because CO_2 can migrate through them under the influence of strong buoyancy forces. This can occur for caprocks with permeabilities as low as $k > 10^{-18}$ m^2 [28]. The permeability of the caprock mainly influences the potential pressure build-up in the caprock and so too the development of fractures. The lower the permeability of the caprock, the less fluid penetration can occur and the less pressure can build up, and, thus, a lower failure risk pertains.

5.2.5. Caprock dip

Caprock dip mainly influences the migration of CO_2 within the reservoir. Due to high buoyancy of the CO_2, the supercritical fluid will tend to move upward in the reservoir until structurally trapped. The greater the caprock dip, the further the CO_2 migrates upwards, with the risk of reaching a spill point or discontinuity in the caprock also increasing. Doughty [29] demonstrates that dipping caprock-storage zone systems lead to preferred CO_2 migration in the up-dip direction. The greater the dip, and its extent, the more quickly, and further, the CO_2 may migrate laterally. Sub-horizontal reservoirs below anticlinal caprock structures, however, form structural traps and therefore securely contain CO_2.

5.2.6. Caprock thickness

As would be expected, thicker caprocks are lower risk for integrity loss, simply because fracture networks and faults can develop further into the caprock without fully transgressing it. For example, at In Salah a fracture network reaches 100-200 m into the caprock [30], but since the caprock package is up to 950 m thick, this has no effect on the security of storage.

5.2.7. Caprock heterogeneity

Caprock heterogeneity increases the risk for integrity and containment loss for various reasons. First, in case of lateral heterogeneity (e.g. in turbidite settings), CO_2 may reach discontinuities in the caprock, which may allow upward migration. In very heterogeneous caprocks, connected fluid pathways to higher strata may be present. Second, heterogeneity of lithology within the caprock may lead to stress concentrations, as has already been discussed with respect to fault boundaries, rendering these interfaces prone to tensile and shear failure.

5.2.8. Number of sealing strata

The number of individual sealing strata within the general caprock package influences the integrity of the system simply by forming a baffled system of multiple storage locations with multiple caprocks which act as buffers if the primary seal below them fails. Rutqvist et al. [21] assessed the risk for caprock failure in multilayered systems. Assessing stress developments in a storage system with three caprocks, of which the lower two have failed, they concluded that ensuing upward migration of CO_2 creates the highest shear and tensional failure risk at the interface of the shallowest storage zone and intact caprock. Thus existence of multiple caprocks is so not a guarantee for CO_2 containment, however, in general the risk for integrity loss decreases with an increasing number of caprocks above the primary intended seal.

5.3. Operations Risk Factors

5.3.1. Well density and number of uncased wells/total number of wells

The number of wells already drilled through the caprock clearly increases the risk of CO_2 migration. The greater the number of wells fully penetrating the caprock and into the storage zone, the greater the number of potential leakage pathways present. Gasda et al. [31] illustrate seven pathways by which CO_2 can leak through previously completed, but now plugged and abandoned wellbores.

5.3.2. Number of uncased wells/total number of wells

The risk of leakage is even greater for uncased wells. Best CO_2 practices currently dictate that new well casings are to be designed to stay intact for timescales on the order of thousands of years. The biggest risk overall for safe CO_2 storage is posed by old abandoned wells, residing mainly in depleted hydrocarbon reservoirs, which were not designed for secure storage for timescales of this magnitude [32].

5.3.3. Temperature difference between injected CO_2 and storage zone

The number of.

5.4. Methodology

For each of the risk factors we establish three order of magnitude risk value ranges corresponding to low, moderate, and high risk. For example, for the first mechanical state risk factor discussed above, the ratio of desired maximum formation pressure to effective minimum horizontal stress, values of 0.5 and below are considered low risk, between 0.5 and .075 moderate risk, and anything higher than 0.75 is considered high risk. Low risk conditions are assigned a risk score of 1. Moderate risk conditions are assigned a risk score of 10. And high risk conditions are assigned a risk score of 100. The purpose for using order of magnitude risk scores is to develop general ranking criteria that are not overly influenced by any one individual factor, many of which are necessarily subjective in nature.

Risk factor scores are assigned to each of the leakage mechanisms (tensile fracture, fault activation, and well damage). If a risk factor does *not* influence a particular leakage mechanism, it is scored as 1 no matter its value. For example, our caprock-storage zone risk factor of caprock permeability clearly has an effect on tensile failure of the caprock, thus a high value for caprock permeability receives a higher risk score. But caprock permeability has no effect on the failure of wellbores or the breeching of older wellbores, so a highly permeable caprock does not influence the well damage mechanism.

We have included 19 factors in QRD4AT and three leakage mechanism for each. Thus each storage site, or potential storage site, receives 57 factor scores. Total risk is the sum of all factor scores, allowing comparison between alternative sites. For each risk factor we have set up ranges that we associated with high, moderate or low leakage potential. Table 2 shows the ranges for separate risk factors.

Table 2 Risk factor value ranges in current QRDAT version

Risk factor	**Risk factor value ranges**		
	High risk	**Moderate risk**	**Low risk**
Lateral extension of the storage zone/formation depth	<25	25-100	>100
Storage zone thickness/storage zone depth	> 0.5	0.1-0.5	< 0.1
Stress regime	Compressional	Transform	Extensional
Caprock strength	Weak	Moderate	Strong
Caprock thickness	≤ 3 m	3-30 m	≥ 30 m
Fault boundaries	Multiple	One	None
Natural seismicity	High	Moderate	Low
Number of caprocks	No	One	Multiple
Maximum formation pressure/formation depth	≥ 0.75	0.625-0.75	≤ 0.625
Desired maximum formation pressure/discovery pressure	≥ 1.5	1.25-1.5	≤ 1.25
Well density	> 15	5-15	< 5
Number of uncased wells/total number of wells	> 0.6	0.2-0.6	< 0.2
Temperature difference between the injected CO_2 and the ambient storage zone temperature	≥ 60 ◦C	30-60 ◦C	≤ 30 ◦C
Caprock heterogeneity	Significant	Moderate	Strong
Caprock permeability	> 10^{-15} m^2	10^{-18}-10^{-15} m^2	< 10^{-18} m^2
Caprock lateral extend/storage zone thickness	<25	25-100	>100
Caprock dip	≥ 8°	2°-8°	≤ 2°
Minimum horizontal stress/vertical stress (stress ratio)	<0.55	0.55-0.65	>0.65

MECHANICAL STATE	tens frac		fault reac		well fail	
1. STRESS						
Max P/min princ stress						
a. ≥ 0,75	0	100	0	100	0	100
b. 0,5-0,75	1	10	1	10	1	10
c. ≤ 0,5	0	1	0	1	0	1
Stress regime						
a. Compressional	1	100	1	100	1	100
b. Transform	0	10	0	10	0	10
c. Extensional	0	1	0	1	0	1
Shmin/Sv						
a. < 0.55	0	1	0	100	0	100
b. 0.55-0.65	0	1	0	10	0	10
c. > 0.65	1	1	1	1	1	1
2. PRESSURE						
Desired Max P/Discovery P						
a. ≥ 1.5	0	100	0	100	0	100
b. 1.25-1.5	0	10	0	10	0	10
c. ≤ 1.25	1	1	1	1	1	1
Max P/formation depth						
a. ≥ 0.75	0	100	0	100	0	100
b. 0.625-0.75	0	10	0	10	0	10
c. ≤ 0.625	1	1	1	1	1	1
3. FAULTS						
Fault boundaries						
a. Multiple bounding faults	1	1	1	100	1	100
b. One bounding fault	0	1	0	10	0	10
c. None	0	1	0	1	0	1
Natural seismicity						
a. High	1	100	1	100	1	100
b. Moderate	0	10	0	10	0	10
c. Low	0	1	0	1	0	1

Fig. 30. Mechanical state risk factors and ranges included in risk assessment tool.

CAPROCK-STORAGE ZONE SYSTEM	tens frac		fault reac		well fail	
4. STORAGE ZONE SPECIFIC						
Lateral extent/storage zone depth						
a. <25	1	100	1	100	1	100
b. 25-100	0	10	0	10	0	10
c. >100	0	1	0	1	0	1
Storage zone thickness/storage zone depth						
a. > 0.5	0	100	0	100	0	1
b. 0.1-0.5	0	10	0	10	0	1
c. < 0.1	1	1	1	1	1	1
5. CAPROCK SPECIFIC						
Caprock heterogeneity						
a. Significant	1	100	1	100	1	1
b. Moderate	0	10	0	10	0	1
c. Low	0	1	0	1	0	1
Caprock strength						
a. Weak	0	100	0	100	0	100
b. Moderate	1	10	1	10	1	10
c. Strong	0	1	0	1	0	1
Caprock thickness						
a. ≤ 3m	0	100	0	100	0	1
b. 3-30 m	1	10	1	10	1	1
c. ≥ 30 m	0	1	0	1	0	1
Caprock lateral extent/caprock thickness						
a. <25	1	100	1	100	1	100
b. 25-100	0	10	0	10	0	10
c. >100	0	1	0	1	0	1
Caprock permeability						
a. k > 1E-15 m2	0	100	0	1	0	1
b. 1E-18 m2 ≤ k ≤ 1E-15 m2	1	10	1	1	1	1
c. k < 1E-18 m2	0	1	0	1	0	1
Number of caprocks						
a. Single	0	100	0	100	0	100
b. Double	0	10	0	10	0	10
c. Multiple	1	1	1	1	1	1
Caprock dip						
a. γ ≥ 8°	1	1	1	100	1	1
b. 2°≤γ≤8°	0	1	0	10	0	1
c. γ ≤ 2°	0	1	0	1	0	1

Fig. 31. Caprock and storage zone risk factors and ranges included in risk assessment tool.

OPERATIONS						
	tens frac		fault reac		well fail	
6. OPERATIONS						
Well density						
a. > 15 km-2	0	1	0	1	0	100
b. 5-15 km-2	0	1	0	1	0	10
c. < 5 km-2	1	1	1	1	1	1
No. of uncased wells/total no. of wells						
a. > 0.6	0	1	0	1	0	100
b. 0.2-0.6	0	1	0	1	0	10
c. < 0.2	1	1	1	1	1	1
ΔT between CO2 and storage zone						
a. ≥ 60 °C	0	100	0	100	0	1
b. 30 °C - 60 °C	1	10	1	10	1	1
c. ≤ 30 °C	0	1	0	1	0	1

Fig. 32. Operating parameters risk factors and ranges included in risk assessment tool.

5.5. *Sample application to five storage projects*

We have applied the risk assessment to evaluate five CO_2 injection and potential injection sites. The first three are potential CO2 sites under consideration, including the Kevin Dome site, the Louden site, and the Wilmington graben. Two others are actual large scale CO2 injection sites, including Sleipner in the North Sea and In Salah in North Africa. The resulting total risk scores are presented in Figure 33.

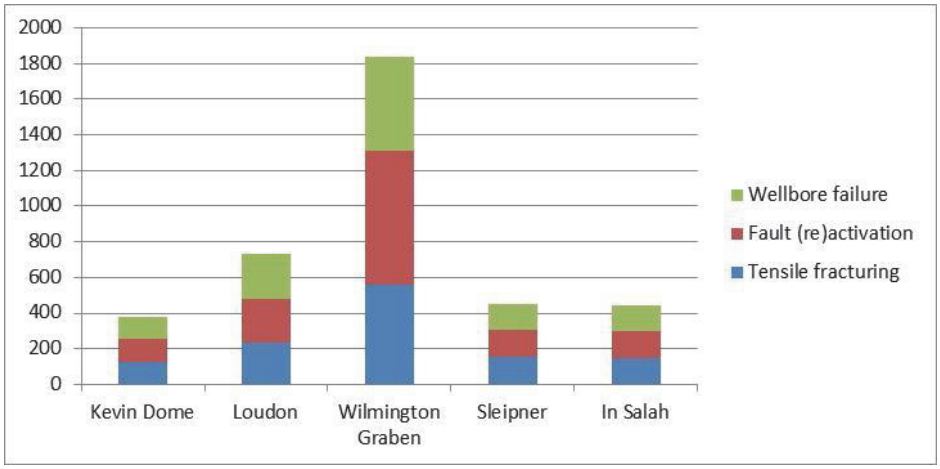

Figure 33 Total QRDAT risk scores for five CO_2 potential and actual injection sites.

Table 3 shows the risk scores for the five locations, including the category scores for the three leakage mechanisms: mechanical state, caprock-reservoir system and operations. The likelihood scores for each site may then be converted to absolute order-of-magnitude probability. An example is provided in Table 4Table 4, and is applied and shown in Fig. 34. The resulting order-of-magnitude probability showed that both the Loudon and Wilmington Graben have a relatively high 10^{-1} risk values, while the other three site examples have relatively moderate 10^{-2} risk

values. Note that these leakage risk ranges are generally consistent with the historical observations of leakage risk in the natural gas storage industry, as discussed earlier in this paper. Also note that of the two actual operating examples, In Salah experienced out of zone fracture concerns and has been shut-in.

Table 3 Estimated Site Risk Scores

Category	Range of risk scores	Kevin Dome	Loudon Field	Wilmington Graben	Sleipner	In Salah
Mechanical State	21-1902	345	660	840	102	390
Caprock-Reservoir System	27-2007	27	45	972	342	27
Operations	9-405	9	27	27	9	27
TOTAL	57-4314	381	732	1839	453	444

Table 4: Relative Risk Scores and Order-of-Magnitude Probabilities

Relative Ranking Score Value	Loss Event Probability Order-of-Magnitude Value
greater than 500	10^{-1}
301 – 500	10^{-2}
201 – 300	10^{-3}
101 – 200	10^{-4}
Less than 100	10^{-5}

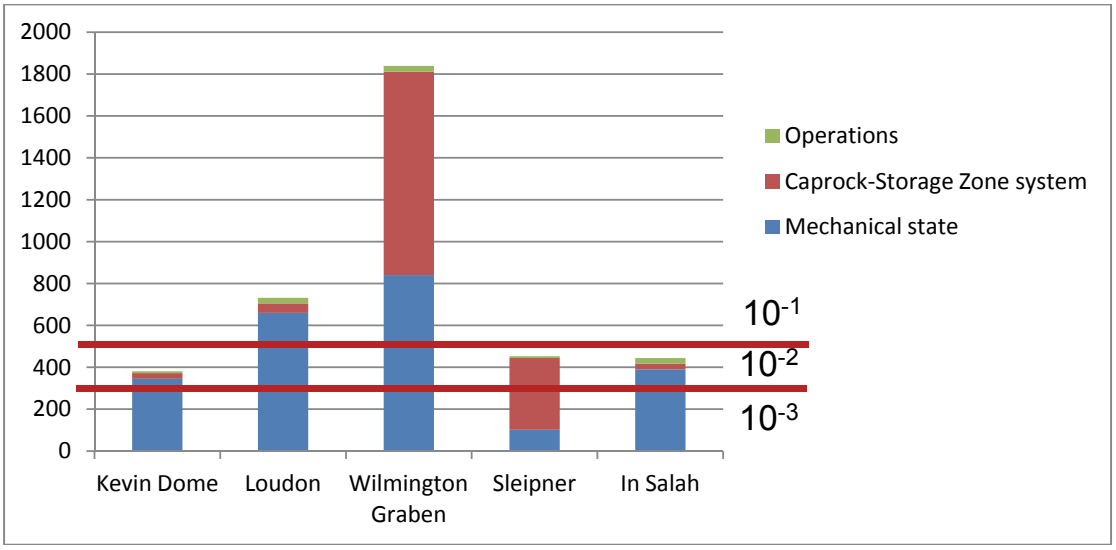

Fig. 34. Relative risk scores and the contribution of the three main groups of risk scores to the relative risk ranking

6. Summary and Conclusions

As part of GeoMechanics Technologies' DOE-funded project, *Development of Improved Caprock Integrity and Risk Assessment Techniques,* we have completed a multi-phase geomechanical caprock integrity study to advance understanding of caprock integrity issues associated with large scale CO_2 injection. First, from our detailed review, analysis, and description of historical leakage events related to caprock integrity within the natural gas storage industry, we conclude that risks for gas leakage events are generally higher than previously estimated and published, and are in the range of 10^{-1} to 10^{-2}. Second, coupled transport flow and geomechanical simulations of three large-scale geologic sequestration sites were completed to analyze their potential of caprock failure due to geomechanical damage. Induces stresses in each of the fields investigated are not sufficient to raise concerns regarding caprock fracturing or fault activation. Third, we have developed and documented a quantitative risk and decision analysis tool to assess caprock integrity risks. Application to five study sites indicates that the Kevin Dome site presents the least risk for CO_2 injection, while the Wilmington Graben site present the highest risk.

Acknowledgements

This material is based upon work supported by the Department of Energy under Award Number DE-FE0009168.

References

[1] Benson SM. Lessons learned from natural and industrial analogues for storage of carbon dioxide in deep geologic formations. LBNL #51170, technical report for BP-DOE CRADA under contract DE-AC03-76F00098; 2002.
[2] Intergovernmental Panel on Climate Change (IPCC). Carbon dioxide capture and storage:summary for policymakers and technical summary. ISBN 92-9169-119-4; 2005.
[3] Perry KF. Natural gas storage industry experience and technology:potential application to CO_2 geological storage. In Benson SM, editor. Carbon dioxide capture for storage in deep geologic formations - results from the CO_2 Capture Project, v. 2:Geologic storage of carbon dioxide with monitoring and verification, London:Elsevier; 2005, p. 815-825.
[4] US Energy Information Administration (EIA). Lower 48 States Natural Gas Working Underground Storage. Accessed 3/11/2013. World Wide Web Address:www.eia.gov/dnav/ng/hist/nw_epg0_sao_r48_bcfw.htm
[5] US Energy Information Administration (EIA). U.S. Underground Natural Gas Storage Capacity. Accessed 3/11/2013. World Wide Web Address:http://www.eia.gov/dnav/ng/ng_stor_cap_dcu_nus_m.htm
[6] Lewicki JL, Birkholzer J, Tsang C. Natural and industrial analogues for leakage of CO_2 from storage reservoirs:identification of features, events, and processes and lessons learned. Environ Geol 2006; Vol. 52, Nos. 3, p, *457-467.*
[7] Burton EA, Myhre R, Myer L, Birkinshaw K. Geologic carbon sequestration strategies for California, The Assembly Bill 1925 Report to the California Legislature. California Energy Commission, Systems Office. CEC-500-2007-100-SD; 2007.
[8] Myer, L. CCS safety and analogues. International seminar on perspectives for near term CCS deployment and capacity building for emerging economies. Porto Alegre, Brazil, October 17–19, 2007. Accessed 3/11/2013. World Wide Web Address:http://www.cslforum.org/documents/9_CCSSafetyAnaloguesMyerOct182007.pdf
[9] Det Norske Veritas (DNV). CO_2QUALSTORE:Workbook with examples of applications. DNV report
No. 2010-0254. Hovik, Norway:Det Norske Veritas AS; 2010. Accessed 3/11/2013. World Wide Web Address:http://www.dnv.com/binaries/CO_2QUALSTORE_Workbook_tcm4-436659.pdf
[10] Evans DJ. A review of underground fuel storage events and putting risk into perspective with other areas of the energy supply chain. Geol Soc Spec Publ 2009;313:173–216.
[11] US Energy Information Administration (EIA). U.S. Underground natural gas storage developments:1998:2005. Office of Oil and Gas, October 2006. Accessed 3/11/2013. World Wide Web Address:http://www.eia.doe.gov/pub/oil_gas/natural_gas/feature_articles/2006/ngstorage/ngstorage.pdf
[12] Katz DL. Containment of gas in storage fields, in SPE Reprint Series 1999; No. 50, 28-33.
[13] Katz DL, Coats KH. Underground storage of fluids, Urich's Books, Ann Arbor, MI, 1968.
[14] Evans DJ, West JM. An appraisal of underground gas storage technologies and incidents, for the development of risk assessment methodology. HSE Research Report RR605. Norwich, UK:Crown, 2008.
[15] Keeley D. Failure rates for underground gas storage:significance for land use planning assessments. HSE Research Report RR671. Norwich, UK:Crown, 2008.
[16] Gor GY, Elliot, TR, Prévost JH. Effects of thermal stresses on caprock integrity during CO_2 storage. International Journal of Greenhouse Gas Control2013; 12, 300-309.
[17] Big Sky Carbon Sequestration Partnership, acquired via personal communication.

[18] Bennion B, Bachu S. Relative permeability characteristics for supercritical CO2 displacingwater in a variety of potential sequestration zones in the Western Canada Sedimentary Basin.Paper SPE 95547 presented at the SPE Annual Technical Conference and Exhibition, Dallas, 9-12October 2005. DOI: 10.2118/95547-MS.
[19] Bachu S, Bennion B. Effects of in situ conditions on relative permeability characteristics ofCO2-brine system. Environ Geol 2008; 54(8):1707-1722
[20] Rutqvist J, TsangCF. A study of caprock hydromechanical changes associated with CO_2-injection into a brine formation. Environ Geol 2002; 42(2-3), 296-305.
[21] Rutqvist J, Birkholzer JT, Tsang CF. Coupled reservoir–geomechanical analysis of the potential for tensile and shear failure associated with CO_2 injection in multilayered reservoir–caprock systems. International Journal of Rock Mechanics and Mining Sciences 2008; 45(2), 132-143.
[22] Mazzoldi A, Rinaldi AP, Borgia A, Rutqvist J. Induced seismicity within geological carbon sequestration projects: maximum earthquake magnitude and leakage potential from undetected faults. International Journal of Greenhouse Gas Control 2012; 10, 434-442.
[23] Rutqvist J, Rinaldi A P, Cappa F, Moridis G J. Modelling of fault reactivation and induced seismicity during hydraulic fracturing of shale-gas reservoirs. Journal of Petroleum Science and Engineering 2013; 107, 31-44.
[24] Sibson RH. Stress switching in subduction forearcs: Implications for overpressure containment and strength cycling on megathrusts. Tectonophysics 2013; 600, 142-152.
[25] Orlic B, ter Heege J, Wassing BBT. Assessing the short-term and long-term integrity of top seals in feasibility studies of geological CO_2 storage. In 45th US Rock Mechanics/Geomechanics Symposium. American Rock Mechanics Association; January 2011.
[26] Rutqvist J, Vasco DW, Myer L. Coupled reservoir-geomechanical analysis of CO_2 injection and ground deformations at In Salah, Algeria. International Journal of Greenhouse Gas Control 2010; 4(2), 225-230.
[27] Vilarrasa V, Olivella S, Carrera J. Geomechanical stability of the caprock during CO_2 sequestration in deep saline aquifers. Energy Procedia 2011; 4, 5306-5313.
[28] Zhou Q, Birkholzer JT, Tsang CF, Rutqvist J. A method for quick assessment of CO_2 storage capacity in closed and semi-closed saline formations. Int ernational Journal of Greenhouse Gas Control 2008; 2(4), 626-639.
[29] Doughty C. Investigation of CO_2 plume behavior for a large-scale pilot test of geologic carbon storage in a saline formation. Transport in porous media 2010, 82(1), 49-76.
[30] Verdon JP, Kendall JM, Stork AL, Chadwick RA, White DJ, Bissell RC. Comparison of geomechanical deformation induced by megatonne-scale CO_2 storage at Sleipner, Weyburn, and In Salah. Proceedings of the National Academy of Sciences 2013; 110(30), E2762-E2771.
[31] Gasda SE, Bachu S, Celia MA. Spatial characterization of the location of potentially leaky wells penetrating a deep saline aquifer in a mature sedimentary basin. Environ Geol 2004; 46(6-7), 707-720.
[32] Orlic, B. (2009). Some geomechanical aspects of geological CO_2 sequestration. KSCE Journal of Civil Engineering 2009; 13(4), 225-232.
[33] Ho A, Fokker PA, Orlic B. Caprock Integrity of Deep Saline Reservoirs and Coupled Processes. Netherlands Institute of Applied Geosciences, Utrecht 2005.
[34] Bruno, M.S., Dusseault, M.B., Balaa, T.T., Barrera, J.A. , Geomechanical Analysis of Pressure Limits For Gas Storage Reservoirs, Paper USA-328-5, presented at the North American Rock Mechanics Symposium, *NARMS '98*, June 3-5, 1998.
[35] Bruno, M.S.; DeWolf, G.; Foh, S. (2000), Geomechanical Analysis and Decision Analysis for Delta Pressure Operations in Gas Storage Reservoir, Presented at the American Gas Association Operations Conference, Denver, CO, May7-9